

# Long-term optical spectral monitoring of NGC 7469

Alla I. Shapovalova,<sup>1\*</sup> L. Č. Popović<sup>2,3,4</sup>, V. H. Chavushyan<sup>5</sup>, V. L. Afanasiev<sup>1</sup>,  
D. Ilić<sup>3,4</sup>, A. Kovačević<sup>3,4</sup>, A. N. Burenkov<sup>1</sup>, W. Kollatschny<sup>6</sup>, O. Spiridonova<sup>1</sup>,  
J. R. Valdes<sup>5</sup>, N. G. Bochkarev<sup>7</sup>, V. Patino-Alvarez<sup>5</sup>, L. Carrasco<sup>5</sup> and V. E. Zhdanova<sup>1</sup>

<sup>1</sup>Special Astrophysical Observatory of the Russian AS, Nizhnij Arkhyz, Karachaevo-Cherkesia 369167, Russia

<sup>2</sup>Astronomical Observatory, Volgina 7, 11160 Belgrade 74, Serbia

<sup>3</sup>Department of Astronomy, Faculty of Mathematics, University of Belgrade, Studentski trg 16, 11000 Belgrade, Serbia

<sup>4</sup>Isaac Newton Institute of Chile, Yugoslavia Branch, Volgina 7, Belgrade, Serbia

<sup>5</sup>Instituto Nacional de Astrofísica, Óptica y Electrónica, Apartado Postal 51-216, 72000 Puebla, Puebla, México

<sup>6</sup>Institut für Astrophysik, Georg-August-Universität Göttingen, Germany

<sup>7</sup>Sternberg Astronomical Institute, 119992 Moscow, Russia

Accepted XXX. Received YYY; in original form ZZZ

## ABSTRACT

We present the results of the long-term (20-year period, from 1996 to 2015) optical spectral monitoring of the Seyfert 1 galaxy NGC 7469. The variation in the light-curves of the broad He II  $\lambda 4686\text{\AA}$  H $\beta$  and H $\alpha$  lines, and the continuum at 5100  $\text{\AA}$  and 6300  $\text{\AA}$  have been explored. The maximum of activity was in 1998, and the variability in the continuum and lines seems to have two periods of around 1200 and 2600 days, however these periodicities should be taken with caution because of the red-noise. Beside these periods, there are several short-term (1-5 days) flare-like events in the light-curves. There are good correlations between the continuum fluxes and H $\alpha$  and H $\beta$  line fluxes, but significantly smaller correlation between the He II and continuum. We found that the time-lags between the continuum and broad lines are different for H $\beta$  ( $\sim 20$  l.d.) and H $\alpha$  ( $\sim 3$  l.d.), and that He II also has a smaller lag ( $\sim 2$ -3 l.d.). The H $\alpha$  and H $\beta$  line profiles show a slight red asymmetry, and the broad line profiles did not changed in the 20-year period. Using the lags and widths of H $\alpha$  and H $\beta$  we estimated the central black hole mass and found that it is  $\sim (1 - 6) \cdot 10^7 M_{\odot}$ , which is in agreement with previous reverberation estimates.

**Key words:** galaxies: active – galaxies: quasar: individual (NGC7469) – galaxies: Seyfert – galaxies: quasars: emission lines – line: profiles

## 1 INTRODUCTION

The variability of Type 1 active galactic nuclei (AGNs) seems to be very common and can be used for investigation of the central part of an AGN, especially of the broad line region (BLR) which emits broad emission lines. A BLR of AGNs is expected to be gravitationally bounded by the central supermassive black hole, and consequently the gas in the BLR is expected to be virialized. This, knowing the broad line widths and the BLR dimension (from reverberation studies) can be used for the black hole mass determination (see e.g. Peterson 2014, and references therein). Therefore, the spectral monitoring of Type 1 AGNs with the variable broad emission line and continuum fluxes is very useful, not only for the black

hole mass estimates, but also to explore the variability in the BLR and investigate the nature of the emission gas motion. One of the well-known Type 1 AGNs, that shows a significant variability in the continuum and line spectra, is NGC 746. Its AGN activity has been monitored in different spectral bands (see e.g. Dultzin-Hacyan et al. 1992; Leighly et al. 1996; Pronik et al. 1997; Wanders et al. 1997; Collier et al. 1998; Nandra et al. 1998; Pronik 2009; Pérez-Torres et al. 2009; Artamonov et al. 2010; Doroshenko et al. 2010; Ugolkova & Artamonov 2011; Peterson et al. 2014; Baldi et al. 2015)

NGC 7469 is probably interacting with another galaxy, IC 5283, that is about 60-70 Mpc far away (see, e.g. Marquez & Moles 1994). Around the active nucleus, a bright circumnuclear ring is located at an angular distance of 2.5 arcsec (or  $\sim 1$  kpc) from the nucleus. The stellar ring shows star-forming activity (starburst region, see Wilson et al.

\* E-mail: ashap@sao.ru

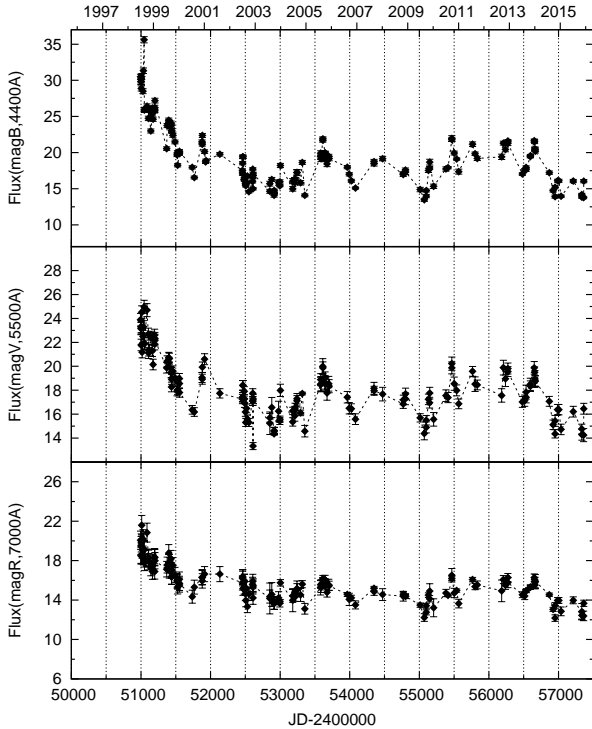


**Figure 1.** Light-curves of the photometry magnitudes in the B, V, R filters, transformed into corresponding fluxes using the equations from [Dietrich et al. \(1998\)](#). The fluxes are given in units of  $10^{-15} \text{ erg cm}^{-2} \text{ s}^{-1} \text{ \AA}^{-1}$ .

1986, 1991; [Díaz-Santos et al. 2007](#); [Izumi et al. 2015](#)), with possible supernova explosions. E.g. the supernova SN 2000ft has been observed in the circumnuclear region in the radio ([Colina et al. 2001](#); [Pérez-Torres et al. 2009](#)) and optical light ([Colina et al. 2007](#))

The spectrum of NGC 7469 shows broad emission lines superposed with strong narrow lines, which is typical for Seyfert 1 galaxies. However, one can in addition expect a contribution of the H II region emission from the star-forming ring.

As was noted above, the AGN of NGC 7469 has been monitored in the X, UV and optical spectral bands. The emission lines ( $\text{H}\beta$  and  $\text{He II } \lambda 4686\text{\AA}$ ) as well as the continuum are variable. However, previous spectral monitoring campaigns covered mostly shorter time periods (of the order of several months). In this paper we present photometric and spectroscopic observations of NGC 7469, with the aim to analyse the long-term variability in the broad lines and continuum fluxes, and in the broad line profiles. For the first time, we present the 20-year long monitoring campaign of NGC 7469.

The paper is organized as following: In section 2 we describe the observations and reduction of observed data, in section 3 we analyse the observed photometric and spectral data and give results, in section 4 the obtained results are discussed, and finally in section 5 we outline our main conclusions.

## 2 OBSERVATIONS AND DATA REDUCTION

### 2.1 Photometry

The BVR photometry of NGC 7469 was performed at the Special Astrophysical Observatory of the Russian Academy of Science (SAO RAS) using the 1-m (1998–2014) and 60-cm (1998–2003) Zeiss telescopes with CCD (530×580) or CCD1K (in 1998–2003) or CCD2K (in 2004–2014). The telescopes are equipped with an offset guided automatic photometer. The characteristics of photometer are given in [Amirkhanian et al. \(2000\)](#) and will not be repeated here. The photometric system is similar to those of Johnson in B and V, and of Cousins in R ([Cousins 1976](#)). We used the software described in [Vlasyuk \(1993\)](#) to reduce the observations. Photometric standard stars from [Penston et al. \(1971\)](#) - in 1998–2003, and from [Doroshenko et al. \(2005\)](#) - in 2004–2015 have been used. These stars are close to NGC 7469, therefore the effects due to differential air mass are negligible for internal calibration purposes. In Table 1 we give the photometric BVR-magnitude. For the light-curves (Fig 1), the magnitudes ( $m(B)$ ,  $m(V)$ ,  $m(R)$ ) were transformed into fluxes  $F(B)$ ,  $F(V)$  and  $F(R)$  in units of  $10^{-15} \text{ erg cm}^{-2} \text{ s}^{-1} \text{ \AA}^{-1}$ , using the equations from [Dietrich et al. \(1998\)](#):

$$\log F(B, \lambda 4400) = -0.4m(B) - 8.180, \quad (1)$$

$$\log F(V, \lambda 5500) = -0.4m(V) - 8.439, \quad (2)$$

$$\log F(R, \lambda 7000) = -0.4m(R) - 8.759. \quad (3)$$

### 2.2 Spectral observations

We monitored the galaxy over a period of 20 years, between June 13, 1996 and July 23, 2015, collecting in total  $\sim 260$  nights of observation. Spectra were acquired with the 6-m and 1-m telescopes of the SAO RAS, Russia (1996–2015), and with the INAOE’s 2.1-m telescope of the “Guillermo Haro Observatory” (GHO) at Cananea, Sonora, México (1998–2007), using a long-slit spectrograph (UAGS in SAO RAS and Boller&Chives in Mexico) equipped with a CCD. The typical wavelength interval covered was from  $\sim 3800 \text{ \AA}$  to  $\sim 7400 \text{ \AA}$  (see Table 3), the spectral resolution was between 8–10  $\text{\AA}$  or 12–15  $\text{\AA}$ , and the signal-to-noise (S/N) ratio was  $S/N > 50$  in the continuum near the  $\text{H}\beta$  line.

Observations with the 1-m SAO RAS telescope have been performed in two modes: 1) using CCD 2K×2K (EEV42-40, 2068×2072 pixels (pxs), 13.5×13.5 mkm), in the wavelength range from 3800  $\text{\AA}$  to 7400  $\text{\AA}$ , with mean spectral resolution of  $\sim 7.5 \text{ \AA}$  and, where both  $\text{H}\alpha$  and  $\text{H}\beta$  lines are covered with one spectrum. The normalization has been performed with the [O III] lines for both lines. The length scale along the slit was 1.35''/px, totally taking 7pxs (9.45''), i.e. the aperture was 4.0''×9.45''; and 2) in the period of 1996–2003 with CCD 1k×1k or 530×580pxs; the slit width was 4.0'' or 8.0'' and the length scale along the slit was 2.2''/px, totally taking 9pxs (19.8''), i.e. the aperture was 4.0''(or 8.0'')×19.8''. The spectral resolution was  $R \sim 8\text{--}10 \text{ \AA}$ . The blue (spectrum around  $\text{H}\beta$ ) and red (spectrum around  $\text{H}\alpha$ ) spectral bands have been observed separately. However they are overlapping at the edges (red edge with blue and *vice versa*) for the wavelength interval of 200–400  $\text{\AA}$ . This has been used for scaling the whole spectrum on [O III] lines.

**Table 1.** The measured photometric magnitudes. Columns are: (1): Number, (2): UT date, (3): Modified Julian date (MJD), (4): Mean seeing in arcsec, and (5)-(7): BRV magnitudes and corresponding errors. The full table is available online.

N	UT-date YYMMDD	MJD 2400000+	Seeing [arcsec]	$M_B \pm \sigma$	$M_V \pm \sigma$	$M_R \pm \sigma$
1	2	3	4	5	6	7
1	980629	50994.00	2.2	13.340 $\pm$ 0.02	12.957 $\pm$ 0.02	12.346 $\pm$ 0.02
2	980706	51001.00	3.2	13.363 $\pm$ 0.02	12.991 $\pm$ 0.02	12.435 $\pm$ 0.02
3	980707	51002.00	3.2	13.351 $\pm$ 0.02	13.057 $\pm$ 0.02	12.430 $\pm$ 0.02
4	980708	51003.00	3.5	13.365 $\pm$ 0.02	12.983 $\pm$ 0.02	12.375 $\pm$ 0.02
5	980709	51004.00	3.2	13.399 $\pm$ 0.02	12.988 $\pm$ 0.02	12.361 $\pm$ 0.02
6	980716	51011.00	2.5	13.339 $\pm$ 0.02	12.929 $\pm$ 0.02	12.267 $\pm$ 0.02
7	980723	51018.00	2.0	-	13.088 $\pm$ 0.02	12.399 $\pm$ 0.02
8	980803	51029.00	2.0	13.413 $\pm$ 0.02	13.022 $\pm$ 0.02	12.339 $\pm$ 0.02
9	980809	51035.00	3.0	13.310 $\pm$ 0.02	12.984 $\pm$ 0.02	12.440 $\pm$ 0.02
10	980819	51045.00	3.5	13.171 $\pm$ 0.02	12.909 $\pm$ 0.02	12.453 $\pm$ 0.02

**Table 2.** Spectroscopic observations information. Columns are: (1): Observatory, (2): Code assigned to each combination of telescope + equipment used throughout this paper, (3): Telescope aperture and spectrograph. (4): Projected spectrograph entrance apertures (slit width $\times$ slit length in arcsec), and (5): Focus of the telescope.

Observatory	Code	Tel.aperture + equipment	Aperture [arcsec]	Focus
1	2	3	4	5
SAO (Russia)	L(N)	6 m + Long slit	2.0 $\times$ 6.0	Nasmith
SAO (Russia)	L(U)	6 m + UAGS	2.0 $\times$ 6.0	Prime
GHO (México)	GHO	2.1 m + B&C	2.5 $\times$ 6.0	Cassegrain
SAO (Russia)	Z1	1 m + UAGS	4.0 $\times$ 19.8	Cassegrain
SAO (Russia)	Z1	1 m + UAGS	8.0 $\times$ 19.8	Cassegrain
SAO (Russia)	Z2K	1 m + UAGS	4.0 $\times$ 9.45	Cassegrain

**Table 3.** Spectroscopic observations log. Columns are: (1): Number, (2): UT date, (3): Modified Julian date (JD), (4): CODE (Code given according to Table 2.), (5): Projected spectrograph entrance apertures, (6): Wavelength range covered, and (7): Mean seeing in arcsec. The full table is available online.

N	UT-date	MJD 2400000+	CODE	Aperture [arcsec]	Sp.range [Å]	Seeing [arcsec]
1	2	3	4	5	6	7
1	13.06.1996	50247.558	L(U)	2.0 $\times$ 6.0	4400-5300	1.1
2	14.06.1996	50248.550	L(U)	2.0 $\times$ 6.0	4400-5300	1.4
3	12.07.1996	50276.535	L(U)	2.0 $\times$ 6.0	3600-5400	1.1
4	13.07.1996	50277.528	L(U)	2.0 $\times$ 6.0	4400-5300	1.6
5	16.07.1996	50280.567	L(U)	2.0 $\times$ 6.0	4400-5300	1.2
6	17.07.1996	50281.576	L(U)	2.0 $\times$ 6.0	3700-7150	2.8
7	25.07.1996	50289.575	L(U)	2.0 $\times$ 6.0	4400-5300	3.6
8	10.08.1996	50305.567	L(U)	2.0 $\times$ 6.0	4400-5300	3.2
9	08.09.1996	50335.447	Z1	4.0 $\times$ 19.8	4140-5800	3.0
10	11.09.1996	50338.422	Z1	4.0 $\times$ 13.5	3890-5450	5.0

If some spectra were poorly corrected for the spectral sensitivity at the ends, for the scaling of the red spectra the doublet [SII] $\lambda\lambda$ 6717,6731 Å has been used.

In the case of the 6-m SAO telescope the spectrograph UAGS (prime focus) or a long slit (Nasmith focus) with the aperture of 2.0'' $\times$ 6.0'' (slit length is 0.4''/px, taking totally 5 pxs). The spectral resolution of this instrument is between 5 Å and 8 Å.

Observations on the 2.1-m (GHO) telescope were made with the aperture 2.5'' $\times$ 6.0'' (scale along slit:  $\sim$  0.46''/px; taking in total 13 pxs). Note here that from 1998 to 2004, the spectral observations were done with a grism of 150 l/mm (a

low dispersion of R=15 Å). From 2004 to 2007, observations obtained with a grism of 300 l/mm (a moderate dispersion of R=8.0 Å) were added. As a rule, the observations were performed with the moderate dispersion in the blue (around H $\beta$ ) or red (around H $\alpha$ ) spectral band during the first night of each set and usually during the next night we used the low dispersion spectrograph covering the whole spectral range from 4000 Å to 7500 Å.

Since the shape of the continuum of active galaxies practically does not change during adjacent nights, it was easy to link together the blue and red spectral bands obtained with the moderate spectral dispersion, using the data obtained for

**Table 4.** Spectral flux scale factor  $\varphi$  and extended source correction  $G(g)$  [in units of  $10^{-15}\text{erg cm}^{-2}\text{s}^{-1}\text{\AA}^{-1}$ ] for different telescopes.

Sample	Aperture (arcsec)	Scale factor ( $\varphi$ )	Extended source correction $G(g)$
Z2K	4.0×9.45	1.000	0.000
Z1	8.0×19.8	1.069±0.024	3.62±0.24
Z1	4.0×19.8	1.017±0.027	1.58±0.74
L(U,N)	2.0×6.0	1.000	-2.0
GHO	2.5×6.0	0.967±0.012	-2.52±0.82

the continuum with the low-dispersion in the whole wavelength range.

Spectrophotometric standard stars were observed every night. Information on the source of spectroscopic observations is listed in Table 2. The log of spectroscopic observations is given in Table 3.

The spectrophotometric data reduction was carried out using either the software developed at SAO RAS (Vlasyuk 1993) or the IRAF package for the spectra obtained in Mexico. The image reduction process included bias and flat-field corrections, cosmic ray removal, 2D wavelength linearization, sky spectrum subtraction, addition of the spectra for every night, and relative flux calibration based on standard star observations. In the analysis, about 10% of the spectra were discarded for several different reasons (e.g. high noise level, badly corrected spectral sensitivity, poor spectral resolution  $>15\text{\AA}$ , etc.). Thus our final data set consisted of 233 blue (covering He II and H $\beta$ ) and 108 red (covering H $\alpha$ ) spectra, taken during 240 nights which we use in further analysis.

### 2.3 Absolute calibration (scaling) of the spectra

The standard technique of the flux calibration based on comparison with the stars of known spectral energy distribution is not precisely enough for studying the AGN spectral variability. Consequently for the absolute calibration, we used fluxes of the narrow emission lines to scale the AGN spectra, since one cannot expect that they vary in a period of tens of years (Peterson 1993). However, recently Peterson et al. (2013) found narrow-line variability in NGC 5548 on a shorter timescale. In the case of NGC 7469 the flux of the [O III] $\lambda$ 5007 $\text{\AA}$  line has not changed noticeably between 1996 (Collier et al. 1998) and 2010 (Peterson et al. 2014), i.e. [O III] $\lambda$ 5007 $\text{\AA}$  flux is in general agreement between two epochs with time distance of 14 years. Therefore we assume that the flux of the [O III] $\lambda$ 5007 $\text{\AA}$  line in NGC 7469 remained constant during our monitoring period (20 years).

All blue spectra of NGC 7469 were thus scaled to the constant flux  $F([\text{O III}]\lambda 5007) = 6.14 \times 10^{-13}\text{erg s}^{-1}\text{cm}^{-2}$  determined by Peterson et al. (2014). The scaling method of the blue spectra have been described in several papers (see Shapovalova et al. 2004, 2010, 2012, 2016, and references therein) and will not be repeated here. This method allows to obtain a homogeneous set of spectra with the same wavelength calibration and the same [O III] $\lambda$ 5007 $\text{\AA}$  flux.

The spectra obtained using the SAO 1-m telescope with the mean resolution of 7.5 $\text{\AA}$  (UAGS+CCD2K, Table 2)

are covering both the H $\alpha$  and H $\beta$  spectral bands. These spectra were scaled using the [O III] $\lambda$ 5007 $\text{\AA}$  line, and the red spectral band was automatically scaled (also by the [O III] $\lambda$ 5007 $\text{\AA}$  flux).

Blue spectra, taken with the 1-m and 6-m telescopes with CCD 1K×1K or 530×580pxs, and with the 2.1-m telescope with a grism of 300 1/mm (Code L(N),L(U),Z1, and GHO from Tables 2 and 3) were also scaled using the [O III] $\lambda$ 5007 $\text{\AA}$  line. In the same night, the scaled blue spectra was merged with the corresponding red spectrum using the overlapping portions of this spectra (see section 2.2). However, the accuracy of the scaling procedure depends strongly on the determination of the continuum slope in the red spectral band, i.e. one has to carefully account the spectral sensitivity of the equipment. This has been performed by using the stars for comparison. In poor photometric conditions (clouds, mist, etc.) the reduction can give a wrong spectral slope (fall or rise) and, consequently, the errors in the scaling procedure for the H $\alpha$  wavelength band can be larger. In the case that only the red spectral band was observed, we used the flux of doublets [S II] $\lambda\lambda$ 6717,6731 $\text{\AA}$  for the absolute calibration. Another source of uncertainty is the fact that the red wing of the [S II] $\lambda$ 6731 $\text{\AA}$  narrow line overlaps with the atmospheric B band (6870 $\text{\AA}$ ), which cannot be properly removed from the end of the red spectral band. Taking all the above facts, we exclude 12 red spectra from the analysis. Most of the H $\alpha$  fluxes have been determined from the spectra that were scaled using the [O III] narrow line. Only 7 red spectra have been scaled using the [S II] $\lambda\lambda$ 6717,6731 $\text{\AA}$  narrow lines.

### 2.4 Unification of the spectral data

In order to investigate the long-term spectral variability of an AGN, it is necessary to gather a consistent and uniformed data set. Since observations were carried out using instruments of different apertures, it is necessary to correct the line and continuum fluxes for these effects (Peterson & Collins 1983). As in our previous papers (Shapovalova et al. 2001, 2004, 2008, 2010, 2012, 2013, 2016), we determined a point-source correction factor ( $\varphi$ ) and an aperture-dependent correction factor to account for the host galaxy contribution to the continuum ( $G(g)$ ), and used the following expressions (see Peterson et al. 1995):

$$F(\text{line})_{\text{true}} = \varphi \cdot F(\text{line})_{\text{obs}}, \quad (4)$$

$$F(\text{cont})_{\text{true}} = \varphi \cdot F(\text{cont})_{\text{obs}} - G(g), \quad (5)$$

where index "obs" denotes the observed flux, and "true" the aperture corrected flux. The spectra of the 1-m telescope+UAGS+CCD2K, within an aperture of 4''×9.45'' were adopted as standard (i.e.  $\varphi=1.0$ ,  $G(g)=0$  by definition). The correction factors  $\varphi$  and  $G(g)$  are determined empirically by comparing pairs of simultaneous observations from each of given telescope data sets to that of the standard data set (as it was used in AGN Watch, see e.g. Peterson et al. 1994, 1998, 2002). The time intervals between observations which have been defined as "nearly simultaneous" are typically of 1–3 days. Note here, that in cases of a higher difference ( $>10\%$ ) between two simultaneous observations (in the 1–3 days interval), which may indicate a fast changing in the flux or some artificial effect, we consid-

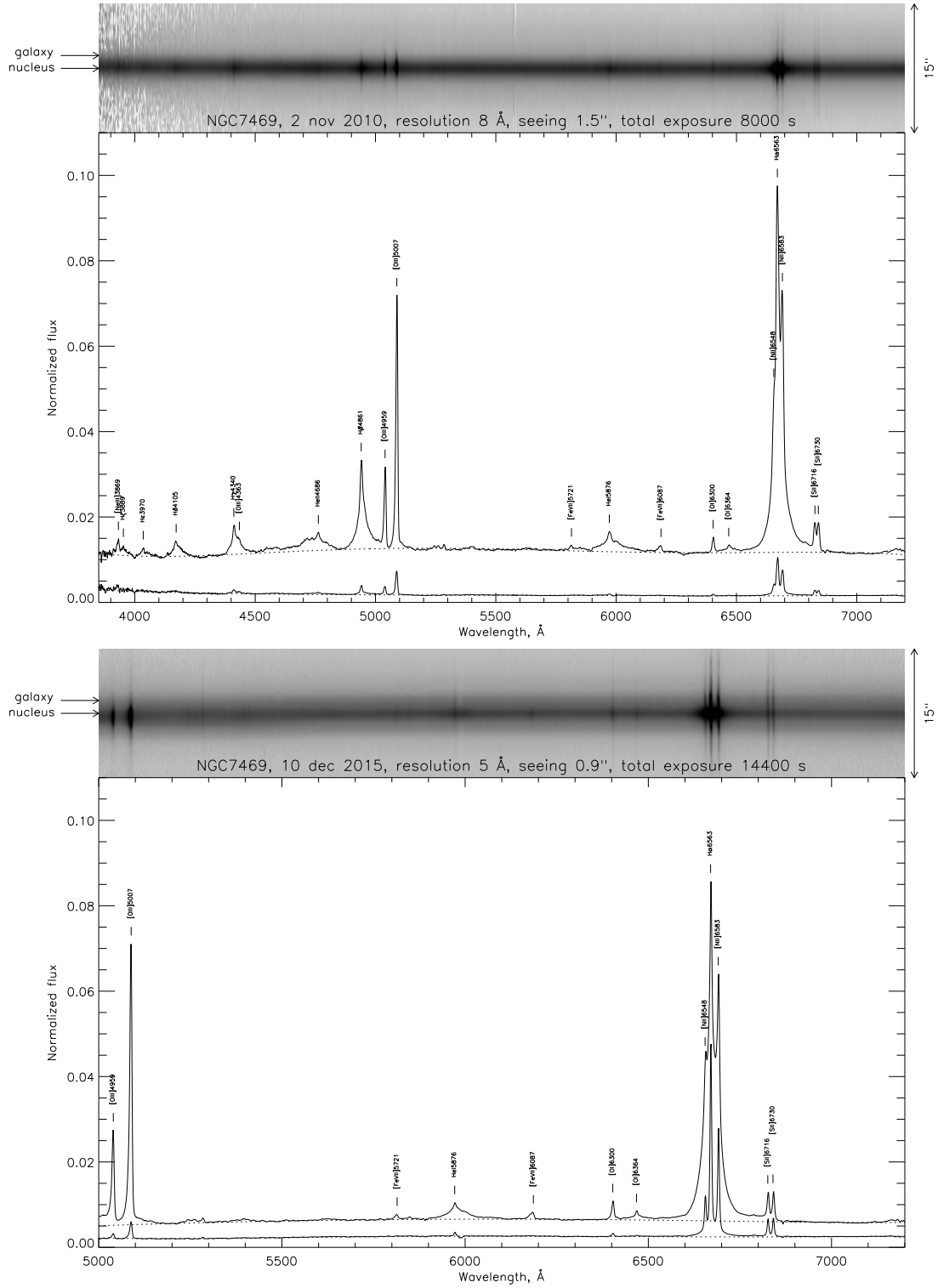


**Figure 2.** Comparison of the AGN to the surrounding stellar-ring emission, using the spectra from two epochs with spectral resolution of 8 Å (upper panel) and 5 Å (bottom panel). The arrows on the spectrum images (top sub-panels) show the positions of the AGN and stellar-ring emission, for which the corresponding spectra are shown below. The strongest emission lines are denoted.

ered them separately (see Sections 2.5 and 3.2.2). The point-source scale correction factor  $\varphi$  and extended-source correction factor  $G(g)$  values (in units of  $10^{-15} \text{erg cm}^{-2} \text{s}^{-1}$ ) for different samples are listed in Table 4.

## 2.5 Flux of the star-forming region vs. the AGN

For the determination of the observed fluxes of  $H\alpha$  and  $H\beta$ , it is necessary to subtract the underlying continuum, which contains, in addition to the AGN continuum, the contribu-

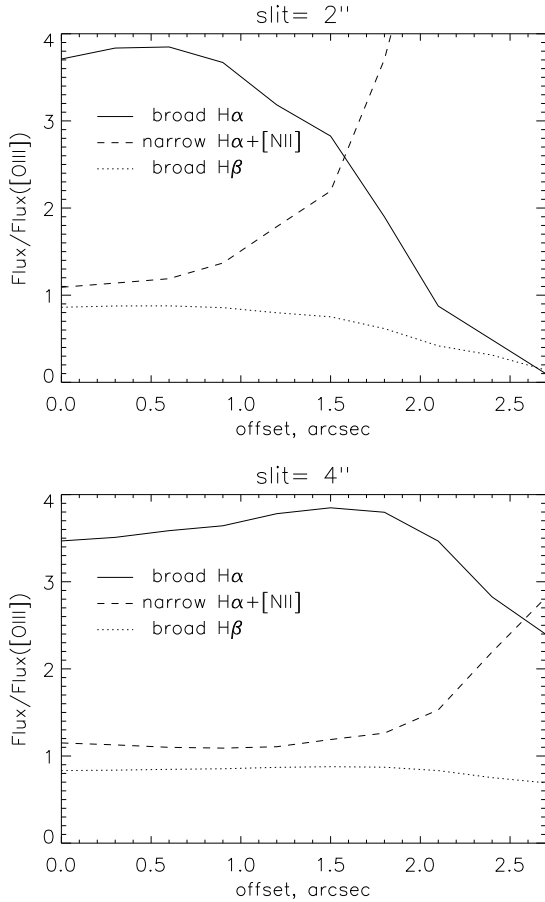


**Figure 3.** Simulation of the slit offset influence on absolute line flux calibration with the [O III] lines, using the slit of 2'' (upper panel) and 4'' (bottom panel). Different lines are denoted on the plots.

tion from the host galaxy and from the star-forming ring around the AGN (see Davies 2004; Díaz-Santos et al. 2007; Rouan & Gratadour 2008). The contribution of the circumnuclear ring can contribute, not only in the continuum emission but also in the narrow lines. Since we used the narrow [O III] lines for absolute calibration (see Section 2.3), the position of the slit, as well as, a small off-centre of the slit can affect our calibration. To check this, we used observations taken with the Spectral Camera with Optical Reducer for Photometric and Interferometric Observations (SCORPIO) spectropolarimeter (the detailed description of the observations will be given in Afanasiev et al. 2016, in preparation).

We have four observations with different position angle of the slit. We show the observations from two epochs with the spectral resolution of 8 Å and 5 Å in Fig. 2. As it can be seen in Fig. 2, there is a contribution of the circumnuclear ring emission in the narrow lines and in the continuum. We accepted that the contribution of the circumnuclear ring and host galaxy in the continuum is  $F_{gal.} = (8.7 \pm 0.9) \cdot 10^{-15} \text{ erg cm}^{-2} \text{ s}^{-1} \text{ Å}^{-1}$  given by Benz et al. (2013). The contribution of the circumnuclear ring to the narrow lines is not significant, especially in lower resolution spectra (see Fig. 2, upper panel).

However, a slight slit motion across the AGN and sur-

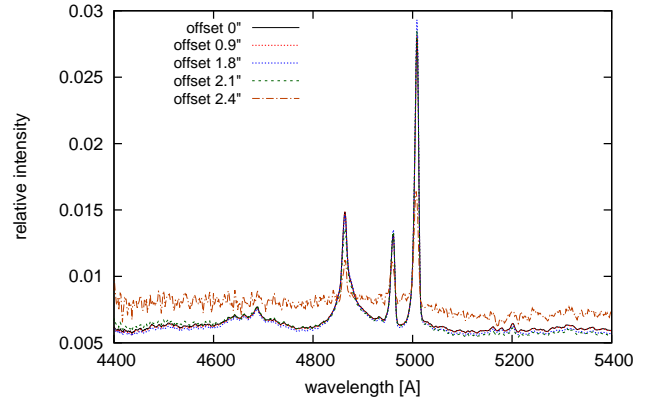


**Figure 4.** Simulations of the observed spectra in the H $\beta$  spectral region (normalized to the [O III] lines) with different slit offsets (denoted in the upper left corner).

rounding stellar ring may be present, and it can affect the intensity of the [O III] lines, and consequently give an artificial broad line variability. To test this, we explore the influence of the slit position to the calibration of the spectra using the [O III] lines. We simulated the influence of the slit of 2'' (see Fig. 3, upper panel) moving across the field (presented in Fig. 2, upper spectrum image on panels), first taking that the AGN is in the centre (see arrows showing the AGN emission) and moving to the offset until 2.5''. We measured the broad H $\alpha$  and H $\beta$ , and narrow H $\alpha$ + [N II] fluxes in the units of the [O III] lines. With such narrow slit, for offset  $>1.0''$  we have a big influence of the slit position to the calibration of the line fluxes. Around 40% of our spectra were obtained with the slit width of 2'' (6-m telescope) and 2.5'' (2.1-m telescope, see Table 2), but for 60% of our spectra the slit width of 4.0'' or 8.0'' (1-m telescope) was used. Therefore we simulated a slit of 4'' across the field of view, requesting that the AGN emission is in the slit. The result of this simulation is shown in Fig. 3 (bottom panel), where one can see that more-or-less the broad H $\beta$  line has a constant intensity until the high offset of  $<2.0''$ , while the H $\alpha$  line tends to be more sensitive to the slit offset  $>1.0''$ . In Fig. 4 we present the H $\beta$  spectral region (normalized to the flux of [O III] lines) with different offsets in the case of a slit of 4.0''. As can be seen in Fig. 4, until offset of  $\sim 2''$  the H $\beta$  spectral line, normalized to the [O III] lines flux, shows no major change in the line flux and profile (it seems to be within the measured error-bars). But with offset larger than 2'' (see the case of 2.4'' offset in Fig. 4), there is a significant change in the broad line flux, and in the continuum.

From exploration of the above presented slit influence, one can conclude that the slit width of 2.0'' moved only for  $>1''$  from the central position (i.e. the offset  $>1''$ , see Fig 3, upper panel) can produce artificial, "flare-like" changes. If the width of the slit is 4'', one can see a similar phenomenon ("flare-like") in the H $\alpha$  flux for offset of  $>1.0''$  and in the H $\beta$  flux for offset of  $>2''$  (Fig. 3, bottom).

Taking into account the results of the slit motion simulation, we have reanalysed each "flare-like" event by comparing spectroscopic and photometric fluxes (aperture of photometric observations was 15'', i.e. we cannot expect the influence of the slit offset on these observations) and discarded those cases where a "flare-like" event is detected in the spectro-

scopic light-curve, but absent in the photometric one. As a result, we have removed from our analysis 12 spectra with the artificial “flare-like” events.

Taking into account the results of simulations we can conclude that the slit offset has more influence on  $H\alpha$  than on  $H\beta$ , therefore in the further analysis, we will concentrate more on the variability of the  $H\beta$  line.

## 2.6 Measurements of the spectral fluxes and errors

From the scaled spectra (see Sections 2.2 and 2.3) we determined the averaged flux in the continuum near the  $H\beta$  line at the observed wavelength  $\sim 5190 \text{ \AA}$  ( $\sim 5100 \text{ \AA}$  in the rest frame), by averaging fluxes in the spectral range of  $5180\text{--}5200 \text{ \AA}$ . The continuum near the  $H\alpha$  line at the observed wavelength  $\sim 6340 \text{ \AA}$  ( $\sim 6240 \text{ \AA}$  in the rest frame), has been measured by averaging fluxes in the spectral range of  $6330\text{--}6350 \text{ \AA}$ .

To measure the observed fluxes of  $H\beta$  and  $H\alpha$ , it is necessary to subtract the underlying continuum. For this goal, a linear continuum has been fitted through the windows of  $20 \text{ \AA}$  located at  $4870 \text{ \AA}$  and  $5140 \text{ \AA}$  for the  $H\beta$ , and at  $6340 \text{ \AA}$  and  $6970 \text{ \AA}$  for the  $H\alpha$  spectral band. After the continuum subtraction, we defined the observed line fluxes in the following wavelength bands: from  $4880 \text{ \AA}$  to  $5012 \text{ \AA}$  for  $H\beta$  and from  $6550 \text{ \AA}$  to  $6790 \text{ \AA}$  for  $H\alpha$ . A linear continuum for He II has been taken at  $4505 \text{ \AA}$  and  $4860 \text{ \AA}$ . He II fluxes have been measured as fluxes between  $4660 \text{ \AA}$  and  $4840 \text{ \AA}$ .

Using  $\varphi$  and  $G(g)$  factors from Table 4, we re-calibrated the observed  $H\beta$  and  $H\alpha$  fluxes, and their corresponding near-by continuum fluxes to a common scale using the standard aperture of  $4.0'' \times 9.45''$ . In Table 5, the fluxes for the continua at the rest-frame wavelengths at  $5100 \text{ \AA}$  and  $6240 \text{ \AA}$ , as well as the He II,  $H\beta$  and  $H\alpha$  lines and their errors are given. The mean errors (uncertainties) of the continuum fluxes at  $5100 \text{ \AA}$  and  $6240 \text{ \AA}$  as well as of the line fluxes of  $H\beta$ , and  $H\alpha$  are in the interval between  $\sim 2.3\%$  and  $3.8\%$ , while for the He II line is estimated to be  $6.4 \pm 4.4\%$  (see Table 6). The error-bars have been estimated by comparing results from spectra obtained within the time interval that is shorter than 3 days. The flux errors given in Table 5 were estimated by using the mean error given in Table 6.

## 3 DATA ANALYSIS AND RESULTS

### 3.1 Photometry

The measured photometric data in the BVR filters for a circular aperture  $15''$  and the corresponding errors are given in Table 1, and shown in Fig. 1. As it can be seen in Fig. 1, the maximum of activity was observed in 1998. Also there are several noticeable outburst peaks with different brightness amplitudes (Fig. 1). For possible four outbursts in the V-photometric light-curve, we listed basic information in Table 7. As can be seen from Table 7, the outburst amplitude (i.e. the ratio of the maximal to minimal flux -  $F(\text{max}/F(\text{min}))$ ) varies from 1.1 to 1.6 times in intensity. The duration of outbursts (i.e. the times between two minimums) also differs. The most prominent outburst peak

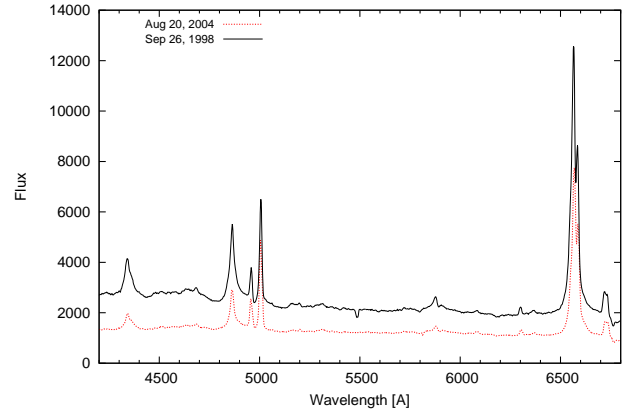


**Figure 5.** Observed spectra in the minimum and maximum of activity during the monitoring period (epoch of observations denoted in the upper left corner).

(number 1 in Table 7), with the highest flux value and duration of  $\sim 1766$  days, seen in Aug 19, 1998 (JD 51045.00). The number 2 and 3 outbursts (durations of 727 and 989 days, respectively), may belong to the same outburst (2+3 in Table 7) that has two peaks in the intensity, which would have total duration of 1716 days. The 4th outburst, with the duration of 1879 days, has 4 small peaks, the intensity of which varies 1.1–1.2 times relative to the neighbouring points. It is very interesting that the duration of outburst number 1, (2+3), and 4 is in the range of  $\sim (1700\text{--}1900)$  days (Table 7), that may indicate periodicity in the flux variability. Further (in Section 3.2.5) we study the possibility of a periodicity in the continuum and line light-curves.

### 3.2 Spectral variability

Fig. 2 shows the spectrum of NGC 7469, where the emission lines are denoted. Beside the Balmer emission lines there are the broad He I  $\lambda 5876 \text{ \AA}$  and He II  $\lambda 4686 \text{ \AA}$ , the broadband features from blended Fe II multiplets at  $\sim 4670 \text{ \AA}$  (Fe II 37 and 38 multiplets) and  $5350 \text{ \AA}$  (Fe II 48 and 49 multiplets)<sup>1</sup>. The broad lines are superposed with their narrow components and the forbidden narrow lines of [O III] $\lambda\lambda 4959, 5007 \text{ \AA}$ , [O I] $\lambda\lambda 6300, 6364 \text{ \AA}$ , [S II] $\lambda\lambda 6717, 6731 \text{ \AA}$ , [Fe VII] $\lambda\lambda 5721, 6087 \text{ \AA}$  etc. The common full width at half maximum (FWHM) of broad lines is  $\sim 2000 \text{ km s}^{-1}$ , and of narrow ones is  $\sim 500 \text{ km s}^{-1}$ , that is typical for Seyfert 1 galaxies. Using the narrow line components we found an average redshift of  $z = 0.0164$  which we accepted as cosmological one. It should be noted that the broad component of He II  $\lambda 4686 \text{ \AA}$  line is very weak in our spectra showing a small flux ( $F(\text{He II}) < 2.0 \times 10^{-13}$ ) compared to Balmer broad lines, and its blue wing is superposed with Fe II  $\lambda 4570 \text{ \AA}$ . In Fig. 5 we present the spectra of NGC 7469 in the minimum and maximum activity during the monitoring period. As can be seen in Fig. 5, there is no big change in the spectral energy distribution between the minimum and maximum states. The continuum flux at  $5100 \text{ \AA}$  decreased by a factor of  $\sim 2$  (see

<sup>1</sup> More details about the optical Fe II lines can be found in Kovačević et al. (2010) and Shapovalova et al. (2012), and also see <http://servo.aob.rs/FeII-AGN/>

**Table 5.** The measured continuum and line fluxes, and their estimated errors. Columns are: (1): Number of spectra, (2): Observed date, (3): Julian Date in [2400000+], (4): Blue continuum, (5): H $\beta$ , (6): Red continuum, (7): H $\alpha$ , and (8): He II. The line fluxes are in units of  $10^{-13}\text{erg cm}^{-2}\text{s}^{-1}\text{\AA}^{-1}$ , and continuum fluxes in units of  $10^{-15}\text{erg cm}^{-2}\text{s}^{-1}\text{\AA}^{-1}$ . The full table is available online.

N	UT-date	JD+	F5100 $\pm \sigma$	F(H $\beta$ ) $\pm\sigma$	F6300 $\pm \sigma$	F(H $\alpha$ ) $\pm\sigma$	F(He II) $\pm\sigma$
1	2	3	4	5	6	7	8
1	13.06.1996	50247.56	14.94 $\pm$ 0.48	8.14 $\pm$ 0.31			2.71 $\pm$ 0.17
2	14.06.1996	50248.55	15.50 $\pm$ 0.50	8.49 $\pm$ 0.32			2.33 $\pm$ 0.15
3	12.07.1996	50276.54	13.54 $\pm$ 0.44	8.00 $\pm$ 0.30			2.04 $\pm$ 0.42
4	13.07.1996	50277.53	14.20 $\pm$ 0.46	8.20 $\pm$ 0.31			2.58 $\pm$ 0.53
5	16.07.1996	50280.57	14.59 $\pm$ 0.47	7.95 $\pm$ 0.30			1.72 $\pm$ 0.35
6	17.07.1996	50281.58	16.41 $\pm$ 0.53	8.01 $\pm$ 0.30			
7	25.07.1996	50289.58	16.94 $\pm$ 0.55	7.50 $\pm$ 0.28			
8	10.08.1996	50305.57	18.73 $\pm$ 0.61	8.14 $\pm$ 0.31			1.52 $\pm$ 0.10
9	08.09.1996	50335.45	19.60 $\pm$ 0.63	8.94 $\pm$ 0.34			
10	11.09.1996	50338.42	18.50 $\pm$ 0.60	9.97 $\pm$ 0.37			
11	12.09.1996	50339.49	19.07 $\pm$ 0.62	9.76 $\pm$ 0.37			
12	02.11.1996	50390.17	18.03 $\pm$ 0.58	11.02 $\pm$ 0.41			3.67 $\pm$ 0.24
13	25.08.1997	50685.55	22.32 $\pm$ 0.72	11.69 $\pm$ 0.44			
14	27.08.1997	50688.45	24.05 $\pm$ 0.78	11.32 $\pm$ 0.42			4.33 $\pm$ 0.28
15	28.08.1997	50689.50	21.83 $\pm$ 0.71	12.05 $\pm$ 0.45			4.04 $\pm$ 0.26
16	30.08.1997	50691.49	22.87 $\pm$ 0.74	12.15 $\pm$ 0.46			4.77 $\pm$ 0.31
17	09.09.1997	50701.45	23.39 $\pm$ 0.76	11.85 $\pm$ 0.44	19.03 $\pm$ 0.57	48.18 $\pm$ 1.12	3.82 $\pm$ 0.24
18	10.09.1997	50702.39	23.68 $\pm$ 0.77	12.19 $\pm$ 0.46	18.87 $\pm$ 0.57	47.68 $\pm$ 1.11	4.11 $\pm$ 0.26

**Table 6.** Estimates of the mean errors for continuum fluxes at 6200 and 5100 $\text{\AA}$ , H $\alpha$ , H $\beta$ , and He II total-line fluxes. Columns are: (1): Measured continuum or line, (2): Observed wavelength range, (3): Rest-frame wavelength range for  $z=0.0164$ , and (4): Estimated error and its standard deviation.

Cnt/Line	Spectral Region [ $\text{\AA}$ ] (obs)	Spectral Region [ $\text{\AA}$ ] (rest)	$\sigma \pm e$ [%]
cont 6200	6330-6350	6228-6248	3.02 $\pm$ 2.41
cont 5100	5180-5200	5096-5116	3.24 $\pm$ 2.30
H $\alpha$ - total	6550-6790	6444-6680	2.32 $\pm$ 1.64
H $\beta$ - total	4880-5012	4801-4931	3.75 $\pm$ 2.75
He II - total	4660-4840	4585-4762	6.41 $\pm$ 4.38

fluxes in Table 5) in the low-activity state, and the slope of the continuum in the blue range was flatter. Besides, the wings of the Balmer lines and the He II line became much weaker than in the high-activity state.

### 3.2.1 Variability of the emission lines and the optical continuum

We analysed flux variability of the emission lines and the optical continuum using 233 spectra of the H $\beta$  line and continuum at 5100  $\text{\AA}$ , 153 spectra of the He II  $\lambda 4686$  line, and 108 spectra of the H $\alpha$  line and red continuum at 6300  $\text{\AA}$ . In Table 5, continuum fluxes of the rest wavelength at 5100  $\text{\AA}$  and 6300  $\text{\AA}$ , and the total H $\beta$ , H $\alpha$ , and He II  $\lambda 4686$  lines are listed. In Fig. 6 the light-curves constructed from the data from Table 5 are presented for the H $\alpha$ , H $\beta$  and He II  $\lambda 4686$  total line fluxes<sup>2</sup> and for the continuum at the rest wavelength  $\sim 5100$   $\text{\AA}$  and 6300  $\text{\AA}$ . For comparison, the first panel

<sup>2</sup> We measured the total line fluxes where both the broad and narrow components are included.

in Fig. 6 shows the photometric light-curve in the V-filter. It can be clearly seen that the spectral variability is following the photometric one. In the light-curves (see Fig. 6) there are several flare-like peaks. These peaks can be either due to the contribution of a ring having a diameter of  $\sim 5''$  ( $\sim 1.6$  kpc) or real flares (details are given in Section 3.2.2).

As usually (see Shapovalova et al. 2008, 2012, 2013, 2016) we estimated the variability rate of the flux in the lines and in the continuum, using the method given by O'Brien et al. (1998). Final light-curve statistics for all five light-curves are given in Table 8. From Table 8 it can be seen that the fluxes in the continuum (at 5100  $\text{\AA}$  and 6300  $\text{\AA}$  rest wavelengths) and the total H $\alpha$  line flux changed for about 2 times, while the H $\beta$  flux was changed  $\sim 3$  times. The highest change is in the He II  $\lambda 4686$   $\text{\AA}$  line, that is about  $\sim 6$  times. The difference in the line flux variations between the H $\alpha$ , H $\beta$  and He II  $\lambda 4686$  lines may be caused by different dimensions of the broad line emitting regions.

We found that the amplitude of variability  $F(\text{var})$  is  $\sim 14\%$  for the continuum and total H $\alpha$  line, and it is larger for the H $\beta$  line ( $\sim 23\%$ ) and He II  $\lambda 4686$   $\text{\AA}$  ( $\sim 32\%$ ).

To explore the variability in the line profiles, we constructed the mean and root-mean-square (rms) line profiles of the H $\alpha$  and H $\beta$  lines (see Fig. 7), averaging separately the continuum subtracted spectra with spectral resolution of  $\sim 8$   $\text{\AA}$  and  $\sim 15$   $\text{\AA}$ . Fig. 7 shows that the broad line profiles (taking the both spectral resolutions) stay similar during the monitoring period<sup>3</sup>. This indicates that the geometry of the line emission regions remain unchanged.

To measure the FWHM of the broad H $\alpha$  and H $\beta$  line components, we fitted the mean profiles of the lines with a number of Gaussian functions using the  $\chi^2$  minimization (see, e.g. Popović et al. 2004) with the aim to subtract the

<sup>3</sup> Note here that the narrow line residuals in Fig. 7 are due to slight difference in the spectral resolution.



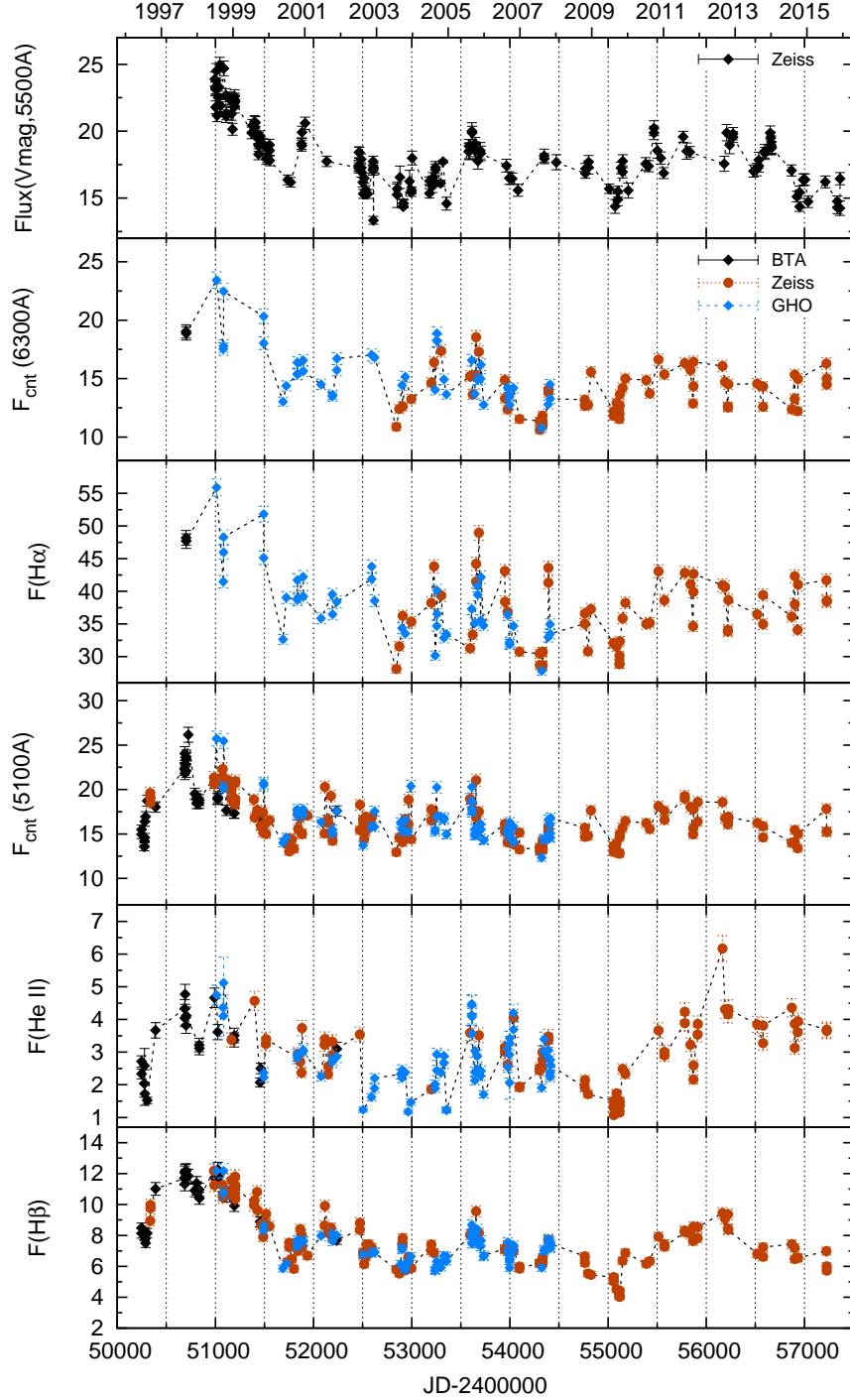


**Figure 6.** Light-curves for the spectral lines and continuum fluxes, compared to the photometry flux in the V filter,  $F(V, \lambda 5500\text{\AA})$  shown in the top plot. Observations with different telescopes are denoted with different symbols shown in the upper two plots. The continuum flux is in units of  $10^{-15}\text{erg cm}^{-2}\text{s}^{-1}\text{\AA}^{-1}$  and the line flux in units of  $10^{-13}\text{erg cm}^{-2}\text{s}^{-1}\text{\AA}^{-1}$ .

contribution of all narrow lines to the mean profiles. As it can be seen in Fig. 8, it seems that broad components of  $H\alpha$  and  $H\beta$  are more complex than can be presented by only one broad Gaussian. There is a very broad component shifted to the red ( $\sim 600\text{ km s}^{-1}$ ). The slightly red asymmetry is present in  $H\alpha$  and  $H\beta$  during the whole monitoring period. Taking only the broad component of the mean profiles (rep-

resented with two broad Gaussian functions - central and one very broad, slightly redshifted, see Fig. 8) we found that the FWHM of the broad  $H\alpha$  component is  $\sim 2100\text{ km s}^{-1}$  that seems to be slightly larger than the FWHM of the broad  $H\beta$  component ( $\sim 2000\text{ km s}^{-1}$ ).

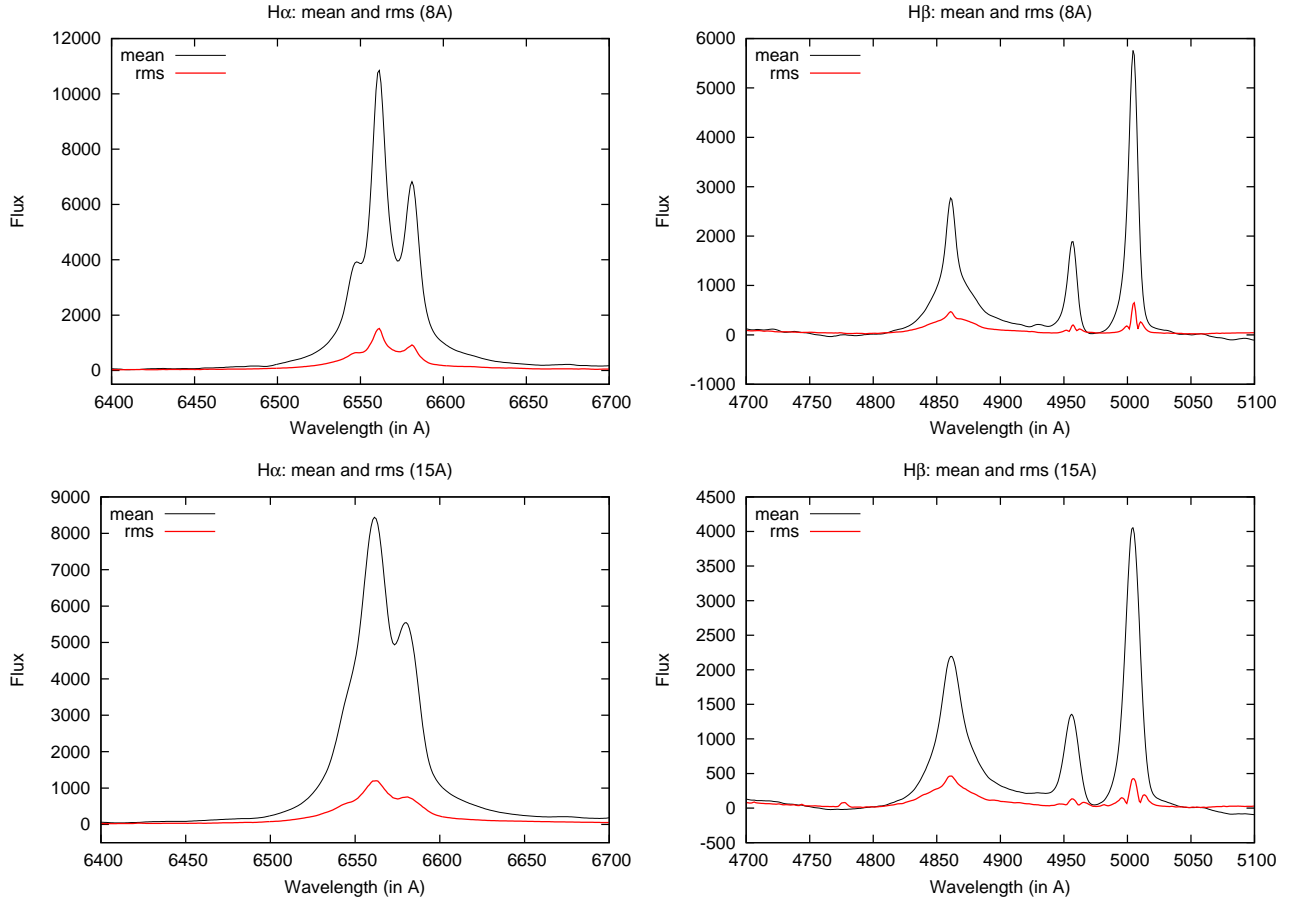


**Figure 7.** Mean and rms profiles of the H $\alpha$  (left) and H $\beta$  (right) lines using spectra with 8 $\text{\AA}$  (upper panels) and 15 $\text{\AA}$  (bottom panels) spectral resolution.

**Table 7.** Outbursts detected in the V-photometric light-curve of NGC 7469. Columns are: (1): Number of flare-like event. (2): UT-date. (3): Modified Julian Date. (4): The V-flux in units  $10^{-15}\text{erg cm}^{-2}\text{s}^{-1}$ . (5): Ratio of the maximal to minimal flux. (6): Difference in days between adjacent minima.

N	UT-date	JD+ 2400000	F(V)	F(max)/F(min)	$\Delta t$ day
1	2	3	4	5	6
1	19.08.1998	51045.00	25.12	1.55	1766
2	30.08.2005	53613.49	20.00	1.38	727
3	06.09.2007	54349.47	18.20	1.20	989
2+3					1716
4	27.09.2010	55467.32	20.42	1.44	1979

### 3.2.2 Flare-like peaks

As noted above (see Section 3.2.1), the light-curves exhibit few flare-like peaks, in which the flux increases for about 10% – 30% in several days. These peaks can be caused both by the contribution from the circumnuclear star-forming ring with the diameter of  $\sim 5''$  (Section 2.5) and by the processes in the AGN which produce flare or flare-like events. In Section 2.5 we discussed that the movement of the slit can con-

**Table 8.** Parameters of the continuum and line variations. Columns are: (1): Analysed feature of the spectrum. (2): Total number of spectra. (3): Mean flux. (4): Standard deviation. (5): Ratio of the maximal to minimal flux. (6): Variation amplitude (see text). Continuum flux is in units of  $10^{-15}\text{erg cm}^{-2}\text{s}^{-1}$  and line flux in units of  $10^{-13}\text{erg cm}^{-2}\text{s}^{-1}$ .

Feature	N	F(mean)	$\sigma(F)$	R(max/min)	F(var)
1	2	3	4	5	6
cont 6300	108	14.64	2.36	2.21	0.158
cont 5100	233	16.78	2.55	2.13	0.149
H $\alpha$ - total	108	37.26	5.42	2.01	0.144
H $\beta$ - total	233	7.99	1.89	3.04	0.233
He II - total	153	2.92	0.94	5.75	0.313

tribute to the artificial flare-like peaks, and consequently we excluded spectra where this was the case. However, in the light-curves we can still see the short flare-like peaks. Unlike the long lasting outbursts observed in the photometric light-curves (of the order of hundreds to thousands days), these events are lasting significantly shorter, of around several (1–5) days. We repeat that we estimated the mean uncertainties in the line and continuum fluxes using observational data, separated by 1–3 days (see Section 2.6), for which we have around  $\sim 5\%$  cases with large difference in the flux ( $\sim 10\%$ – $30\%$ ), indicating flare-like events. As noted before, we ac-

counted the spectroscopic flare-like events, only if we could find the counterpart in the photometric light-curve.

In Table 9 we list some information for the possible flare-like events detected in the spectral light-curves. From Table 9, it can be seen that during the flares, which is lasting between 1 and 3 days, the flux amplitudes vary within 1.1–1.4 times. The most prominent flares, which are seen in the photometric and spectroscopic light-curves are noted as 2 and 3 in Table 7 and denoted as the spectral flares 4 and 5 in Table 9.

Additionally, we examine the measurements of the ratio of the narrow lines that should systematically change in the case of the slit offset effect. For this we first subtracted the underlying continuum (Fig. 9, upper left panel), and then performed the multi-Gaussian best-fitting described in Popović et al. (2004), which includes the Fe II template from Kovačević et al. (2010); Shapovalova et al. (2012) (see Fig. 9, upper right panel), and finally extracted the narrow lines. For the flare-like peak observed in 2005, we found the flux of the narrow lines only, and then we explore if there is a change in the narrow line ratios (Fig. 9, bottom left panel) and in the narrow line ratio as a function of the continuum at 5100 Å (Fig. 9, bottom right panel). Fig. 9 illustrates that there is no trend in the ratio of the narrow lines, which is expected in the slit offset effect. It seems that the flare-like peaks in the NGC 7469 light-curve are real. The nature of the peaks may be that we have some short time outburst which have been detected in other AGNs (see e.g. Shapovalova et al. 2012). Additionally, in the photometric light-curves given in Doroshenko et al. (2010), the presence of flare-like peaks is obvious (see Fig. 1 in their paper).

### 3.2.3 Line and continuum flux correlations

To explore the correlation between lines and corresponding continuum, in Fig. 10 we plot the fluxes of H $\beta$  vs. 5100 Å continuum and H $\alpha$  vs. 6300 Å continuum. Fig. 10 shows that there are good correlations between the line fluxes of H $\beta$ /H $\alpha$  and the corresponding continuum. The correlation coefficients in both cases are quite high ( $r \sim 0.8$ ), indicating that the ionizing continuum is a good extrapolation of the optical one. This is supported by the fact that the correlation between the blue ( $\sim 5100\text{Å}$ ) and the red ( $\sim 6300\text{Å}$ ) continua is very high ( $r \sim 0.94$ , Fig. 11). However, the correlation between the flux of He II  $\lambda 4686\text{Å}$  with the continuum 5100 Å and H $\beta$  is very low (see Fig. 12). This is probably coming from the uncertainties of the He II flux measurements, since the line is very weak, especially in the low state of the AGN activity. Moreover, the He II line is influenced with the Fe II multiplets (see dashed line underneath the observed spectrum in Fig. 9, upper right). Higher scatter of points is seen for lower values of the He II flux (right panel in Fig. 12). Also the correlations between H $\alpha$  vs. H $\beta$  is slightly smaller ( $r \sim 0.73$ , Fig. 11) than their correlation with the continuum. The latter may be due to the fact that, as we noted above (Section 2.6), the H $\alpha$  line can be affected by very small slit position offset.

### 3.2.4 Time-lag analysis

We applied the ZDCF and SPEAR statistical methods to calculate the time delays of continuum and line light-curves.

Detailed description, examination, and comparison of these methods is given in Kovačević et al. (2014). Notice that one of the employed methods (SPEAR) is also used by Peterson et al. (2014) for the same object, but for a set of spectra observed in a much shorter period.

The obtained time-delays are presented in Fig. 13. First we find time-delays using the observed data, and we obtained that ZDCF gives the similar lags for H $\alpha$  and H $\beta$  around 11–12 days, while SPEAR gives larger differences between H $\alpha$  ( $\sim 4$  days) and H $\beta$  ( $\sim 17$  days). An important result of the SPEAR analysis is that the probabilities of the SPEAR time-delays of both curves (see Fig. 13, right panel) clearly show unique peaks. This fact supports the time-lag range of 11–17 days for H $\beta$ , and about 4 times shorter time-lag of H $\alpha$ . From the other hand, the ZDCF and SPEAR time-lags of the He II  $\lambda 4686\text{Å}$  line are in a good agreement with each other as well as with Peterson et al. (2014), giving time-delays of 2–3 days.

Since we have long-term observations covering 20 years and observational gaps, we performed Gaussian process regression (GPR) to generate the light-curves of lines as it is shown in Fig. 14. We found the time-lags using both observed and generated light-curves.

From generated light-curves we obtained time delays as following: for H $\beta$  time-lag is  $23.2^{+5.2}_{-15.0}$  days (SPEAR) and  $21.0^{+7.0}_{-0.0}$  days with cross correlation coefficient of  $0.80^{+0.01}_{-0.01}$  (ZDCF), for H $\alpha$  time-lag is  $3.2^{+0.7}_{-1.0}$  days (SPEAR) and  $3.3^{+9.8}_{-3.3}$  days with cross correlation coefficient of  $0.80^{+0.01}_{-0.01}$  (ZDCF), and for He II time-lag is  $2.5^{+3.2}_{-1.5}$  days (SPEAR) and  $3.5^{+10.5}_{-3.5}$  days with cross correlation coefficient of  $0.44^{+0.03}_{-0.03}$  (ZDCF).

To better assess how the time-lag between the continuum and H $\beta$  line has behaved during the monitored period, we have divided these light curves into two halves (according to the length of the monitored period, the dividing date is JD 2453734.63), and determined time-lags for each of them. For the first part we obtain the ZDCF time-lag of  $15^{+6}_{-1}$  days with cross correlation coefficient of  $0.80^{+0.02}_{-0.02}$ , and the SPEAR time-lag is  $19.4^{+5.0}_{-4.5}$  days. For the second part the ZDCF time-lag is  $28^{+7}_{-1}$  with cross correlation coefficient of  $0.60^{+0.04}_{-0.03}$  and the SPEAR time-lag is  $22.0^{+14.2}_{-9.1}$ . This illustrates that the time-lag for H $\beta$  remains consistent (within the frame of the error-bars) across the monitored period.

Our time-delays for the H $\beta$  and He II lines are quite similar to the ones obtained by Peterson et al. (2014) and, moreover they are within  $3\sigma$  distance (they found time delay of 11–20 days for H $\beta$  and 1–2 days for He II). However, it is interesting that the H $\alpha$  line has a smaller time-lag than the H $\beta$ , and that it is closer to the time-lag of the He II line. This is quite unusual and it seems also unphysical due to following reasons: (i) the H $\alpha$  and H $\beta$  should come from the same emitting gas, and there can be a slight difference between the H $\alpha$  and H $\beta$  lags, but as a rule the H $\alpha$  lag is larger than H $\beta$  one (see Shapovalova et al. 2008, 2010), however the difference should not be too large as in this case; (ii) as it is shown in Section 3.2.1 the H $\alpha$  and H $\beta$  have practically the same FWHM and their different lags indicate that the emitting gas does not follow motion as  $r^{-1/2}$ , i.e. the gas virialization is not present, that is unlikely to happen. Additionally, note here again, that H $\alpha$  is more sensitive to the slit offset than H $\beta$ . Finally, the correlation peaks for both H $\alpha$  and He II are not convincing for both used methods (see

**Table 9.** Possible flares in spectral light-curves of NGC 7469. The columns are: (1): Number of spectral flare-like event. (2): UT-date, (3): Modified Julian Date, (4): Difference in days between the event with the maximal flux and the nearest point (event) on the light-curve, (5-9): Ratio of the maximal flux in the flare to the flux of the nearest point - for continuum at 5100 Å, H $\beta$ , He II 4686 Å, continuum at 6300 Å, and H $\alpha$ , respectively, (10): Modified Julian Date for maximal photometric flare, and (11): Number of photometric flare from Table 7.

N spec.	UT-date	JD+ 2400000 spec.	$\Delta t$ day	F(max)/F(nearest)					JD+ 240000 phot.	N
				5100	H $\beta$	He II	6300	H $\alpha$		
1	2	3	4	5	6	7	8	9	10	11
1	25.10.1998	51083.73	1	1.26	1.13	1.24	1.26	1.05	51045	1
2	24.07.2001	52115.47	3	1.37	1.15	1.05	-	-	52107	
3	06.09.2004	53254.95	1	1.20	1.04	1.20	1.00	1.16	53242	
4	11.10.2005	53655.14	1	1.25	1.20	-	1.21	1.07	53613	2
5	17.10.2007	54391.39	2	1.08	1.01	1.22	1.08	1.25	54349	3
6	12.11.2010	55513.38	$\sim 75$	1.17	1.25	1.22	1.21	1.22	55467	4

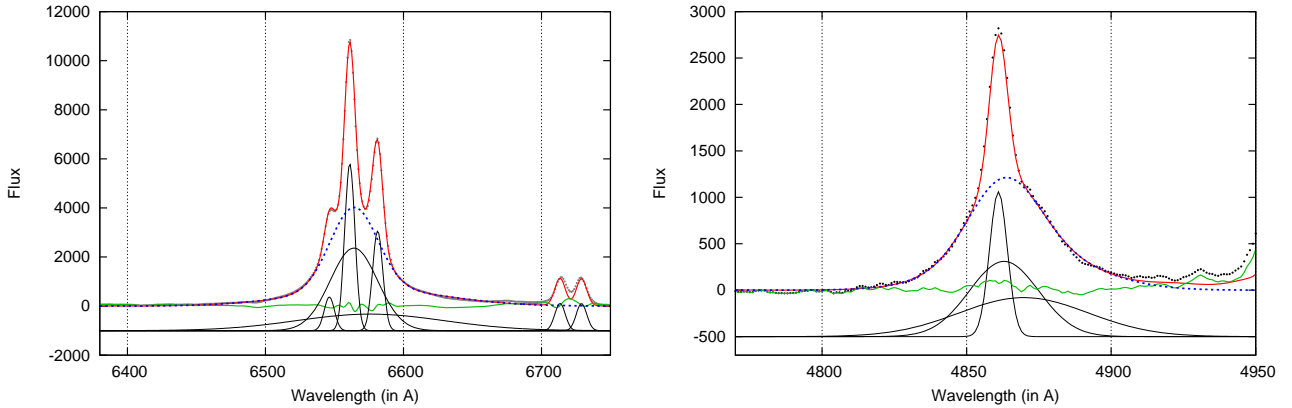


**Figure 8.** The Gauss best-fitting of the mean H $\alpha$  (left) and H $\beta$  (right) lines (dots) of the 8Å spectral resolution (the same as in Fig. 7, upper panels). The model is given with solid line, the modeled broad line component with dashed line, and the residual is shown underneath. The Gaussian components are shown shifted below (solid lines).

Fig. 13) that have the influence on the lag uncertainties for these lines. Therefore, considering the above discussion the obtained time-lags for H $\alpha$  and He II (since we have Fe II contribution) should be taken with caution.

### 3.2.5 Periodicity

A very important and common variability feature in AGN light-curves is red noise, which can lead to relatively dominating peaks in the power spectrum of periodograms at low frequencies. Therefore, it is important to consider possible sources of noise when testing for periodicity in light-curves. Although this type of flux variability is called "red noise", this variability most likely arises from physical processes from the source.

Therefore, in our timing analysis we tested whether a purely red noise model can produce periodic variability of light-curves. For this purpose, all red noise simulations were produced by Ornstein–Uhlenbeck (OU) process (red noise) within the framework of Gaussian process regression model (Rasmussen & Williams 2006). We simulated OU process with a variance of real light-curves. Then we obtained random light-curves from the OU process sampled to a regular time interval. We used them to test that a periodicity of the observed light curves is the product of random variations.

For each observed and modeled light-curve we calculated Lomb–Scargle periodogram with a bootstrap analysis to compute its significance as it is described in Shapovalova et al. (2016).

The periodogram analysis (Fig 15)) shows that there are three possible periods of  $\sim 2600$ , 1700, and 1200 days present in observed data. However, in the H $\alpha$  line, these peaks are not significant, while in the case of the continuum at 6300 Å, the peak of 1700 days is missing. Perhaps this period is not relevant. Moreover, these peaks are presented in random walk simulated data and their power is comparable to those in the observed data, especially in the case of the continuum at 5100 Å (Fig 15). Only in the case of H $\beta$ , two smaller peaks are of greater power than those in red noise simulated data.

Therefore, the possible periods are 2600 and 1200 days, but they must be interpreted with caution because similar periodicities are also prominent in the red noise simulations. Thus, we propose that the detected periodicities are the product of either: i) random variations within the object; ii) the sampling resolution; iii) some periodic process within the core of object, or iv) a combination of all above factors.

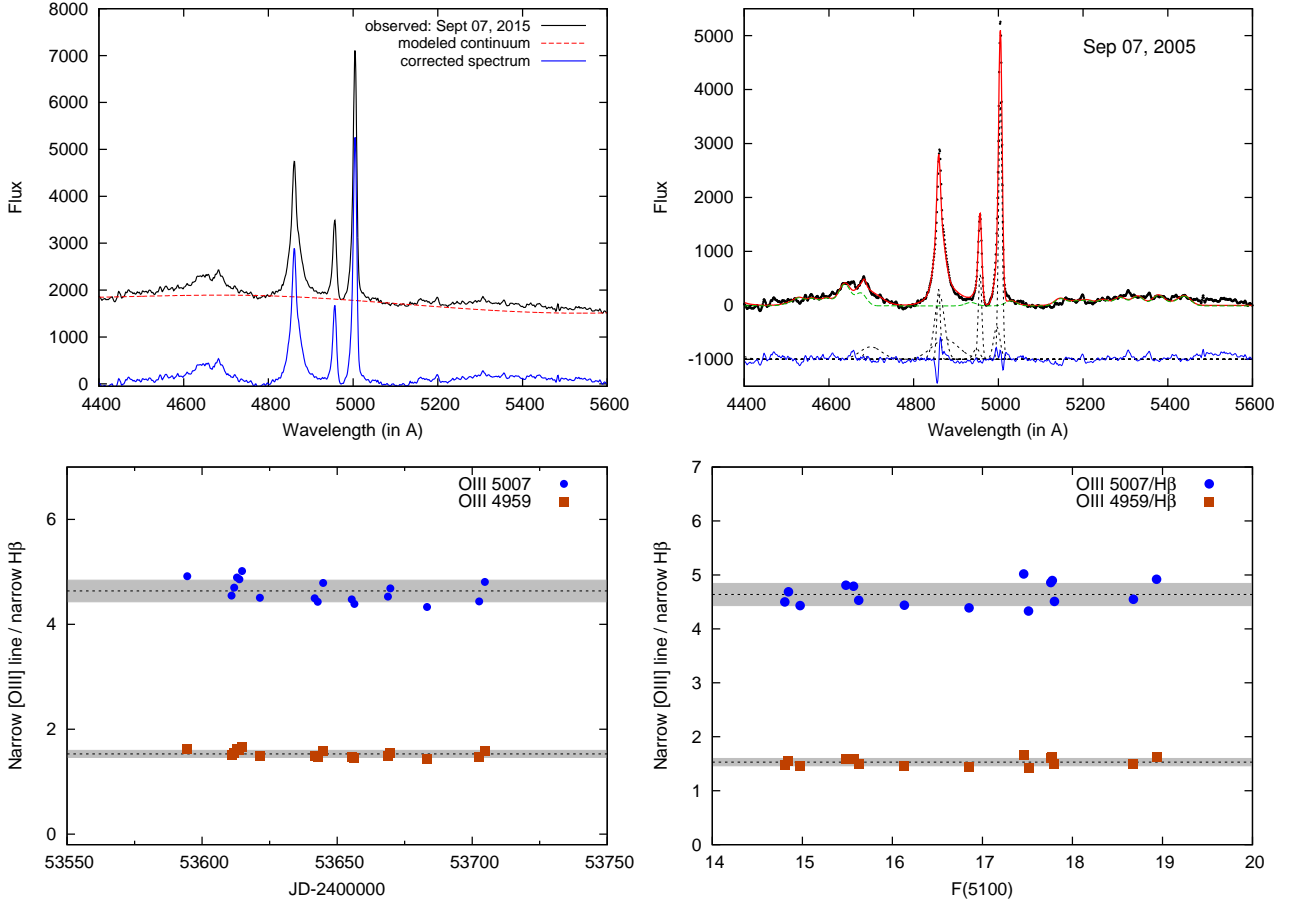


**Figure 9.** Example of the continuum subtraction using cubic spline (upper left) and multi-Gaussian best-fitting (upper right) of the spectral range 4200–5600Å. Below are shown the change of the narrow lines to H $\beta$  narrow line flux ratio during 2005 flare-like event (left) and the narrow-line to H $\beta$  (narrow) line flux ratio vs. continuum flux at 5100 Å (right).

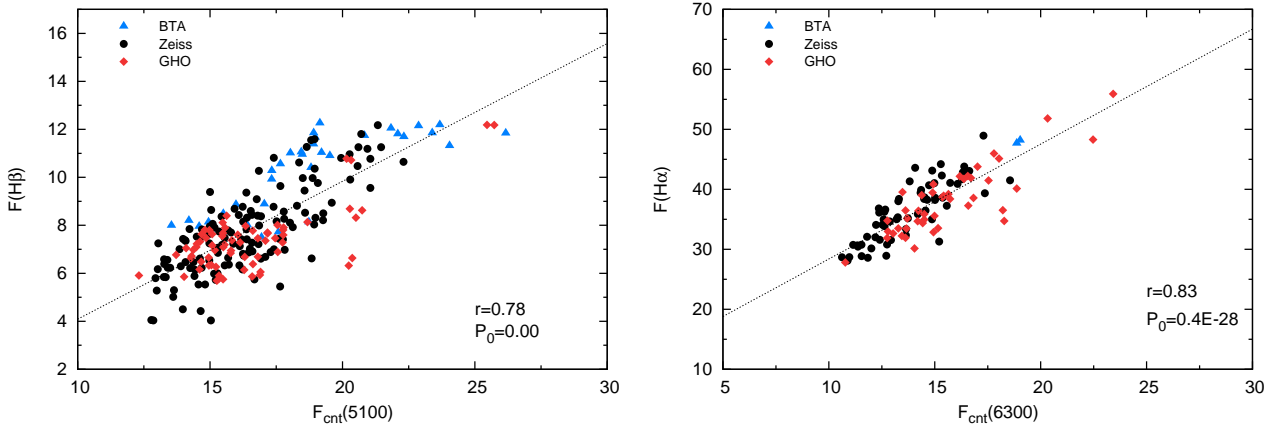


**Figure 10.** Continuum vs. line flux for H $\beta$  (left) and H $\alpha$  (right). Symbols and units are the same as in Fig.6.

#### 4 DISCUSSION

We explore the long-term photometric and spectroscopic variability of the NGC 7469 AGN observed with four telescopes in a common monitoring campaign that lasted for 20 years (from 1996 to 2015). We carefully selected the observed spectra, taking into account that there may be a slit offset

during the observations, in which case the contribution of the stellar circumnuclear ring can affect the continuum and line fluxes. Our measurements are presented in Tables 1 and 5.

The obtained results can be compared and discussed in the frame of previous findings. As we noted above, NGC 7469

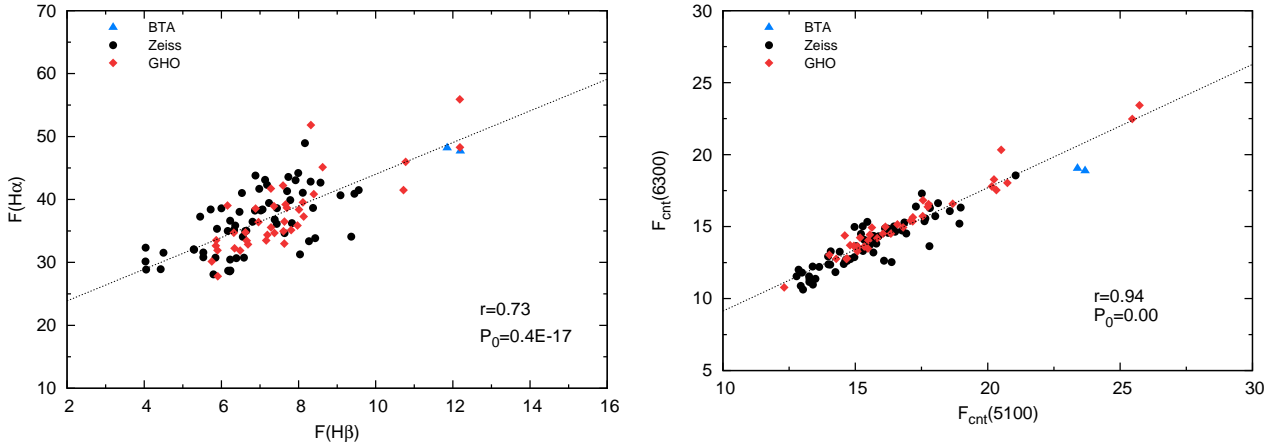


**Figure 11.**  $H\alpha$  vs.  $H\beta$  line flux (left) and red vs. blue continuum flux (right). Symbols and units are the same as in Fig. 6.

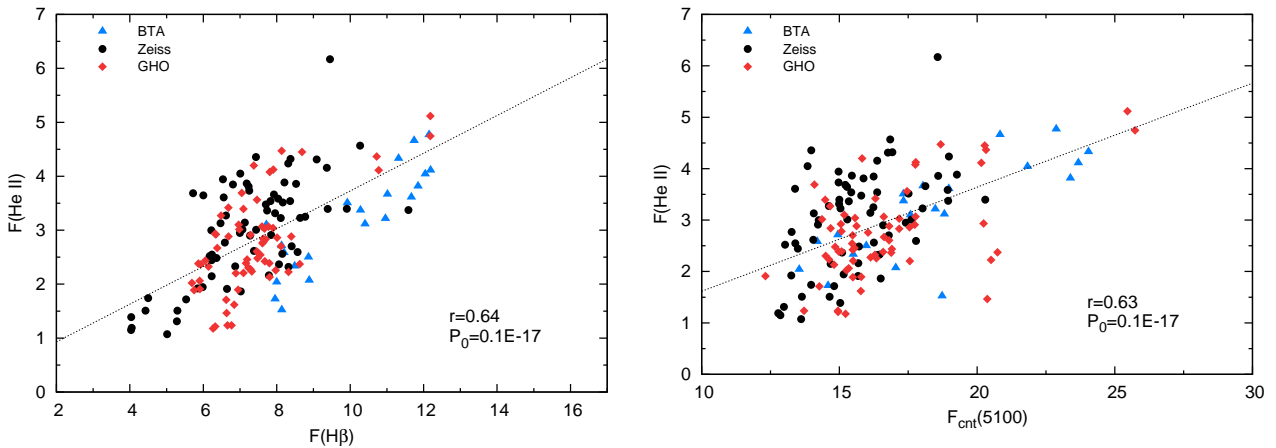


**Figure 12.** He II vs.  $H\beta$  line flux (left) and blue continuum flux (right). Symbols and units are the same as in Fig. 6.

is one of the most observed and investigated type 1 AGNs, from early 60's and 70's (see e.g. Burbidge et al. 1963; Ulrich 1972; Yankulava 1973; Anderson 1973; Pronik 1974, 1975, 1976, etc.). First spectral monitoring campaigns started at the middle of 70's (see Pronik 1974, 1975, 1976) with the aim to investigate changes in the broad lines (mostly in the  $H\beta$  spectral range) and continuum. First spectral observations of NGC 7469 showed rapid variations, with the broad line component almost disappeared (Chuvaev et al. 1990; Pronik et al. 1996, 1997). However, these results have to be taken with caution, since we demonstrated that the slit offset can significantly affect the observed broad line intensities (see Section 2.6).

On the other side, the rapid photometric variability of the nucleus seems to be present and observed (see Dultzin-Hacyan et al. 1992; Lyutyi et al. 1995; Glass 1998; Merkulova 2000; Artamonov et al. 2010), very often as the short-term outburst, which are in support of our finding of flare-like events seen in the photometric and spectroscopic light-curves (see Section 3.2.2).

Reverberation monitoring campaigns (in the X, UV and optical band) started at the end of 90's (Wanders et al. 1997; Collier et al. 1998; Nandra et al. 1998), in which the time delay of different broad lines have been determined, and

some estimates of the central black hole mass were given. The radio-band monitoring for eight years was performed by Pérez-Torres et al. (2009), but was more concentrated on supernova events in the circumnuclear ring. It is interesting that we could not find significant changes in the optical photometric and spectroscopic light-curves after the explosion of SN 2000ft (Colina et al. 2001, 2007) (see Fig. 6). In this period we could not detect an outburst or flare like events.

#### 4.1 Long-term variability – nature of the BLR and continuum source

We performed different CCF analyses to find the time delays between the continua and broad emission lines. The analysis of the obtained results and measurements allows us to discuss the nature of the BLR of NGC 7469.

We found that there are very strong correlations between the  $H\beta$  and  $H\alpha$  line flux variabilities with the corresponding continuum (at 5100 Å and 6300 Å respectively). This is in favour of the classical view of the BLR which is composed from the photoionized gas. Additionally, it was shown before that the UV emission is caused by the reprocessing of the X-rays (see Petrucci et al. 2004). Also, we

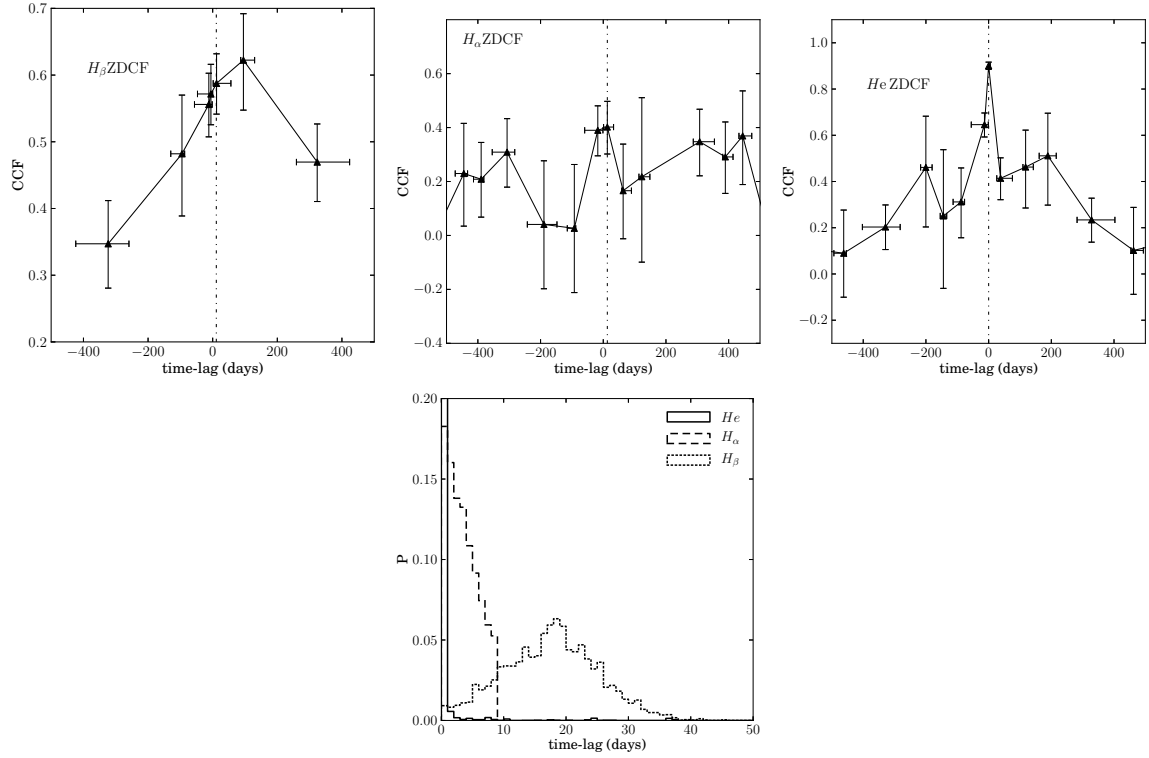


**Figure 13.** Cross correlation functions for the H $\beta$ , H $\alpha$  and He II broad lines. The upper panels show the ZDCF for H $\alpha$ , H $\beta$  and He II, respectively, while on the bottom panel, the SPEAR for three lines is plotted.

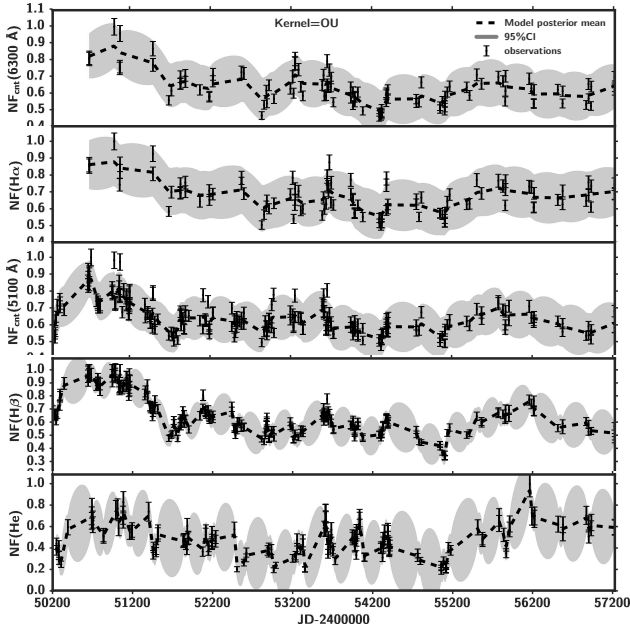


**Figure 14.** Generated light-curves (dashed line) for the continua and broad lines using the Gaussian process regression. Shaded bands represent the 95% confidence interval (CI) for the predicted light-curves.

show in Fig. 16 the H $\alpha$ /H $\beta$  ratio as a function of the continuum at 5100 Å and the 6200Å/5100Å continuum flux ratio. Fig. 16 shows that the H $\alpha$ /H $\beta$  ratio is decreasing with

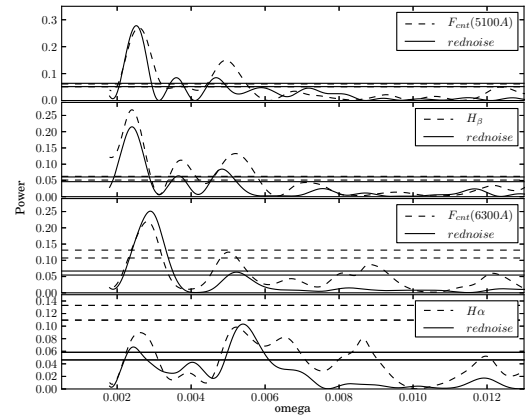


**Figure 15.** Lomb-Scargle periodograms for continua and broad lines original light-curves (dashed lines) and simulated red-noise light-curves (solid lines).

the continuum flux at 5100 Å, but it is increasing with the 6200Å/5100Å continuum flux ratio. This indicates that the broad line ratio are sensitive to the continuum flux, and therefore, the gas in the BLR is most likely photoionized by the central continuum source (accretion disc).

On the other hand, there is a smaller correlation between the flux variation in the He II  $\lambda$ 4686Å line and the continuum at 5100 Å than in Balmer lines. In principle it can be caused by uncertainties in the He II line flux mea-

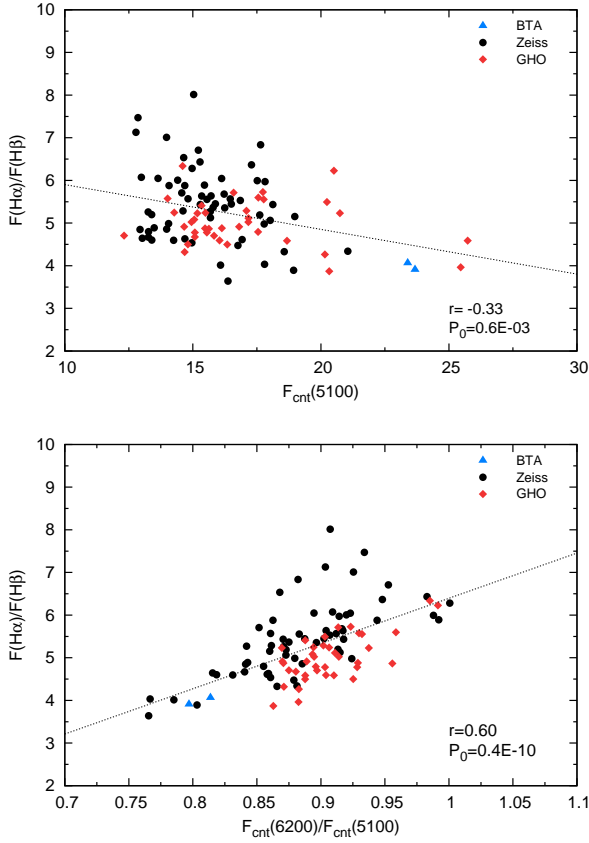


**Figure 16.** The  $H\alpha/H\beta$  flux ratio vs. continuum at  $5100 \text{ \AA}$  (upper) and the  $H\alpha/H\beta$  flux ratio vs.  $6200\text{\AA}/5100\text{\AA}$  continuum flux ratio (bottom). Symbols are the same as in Fig. 6.

measurements, since the line is very weak (especially in the low-activity AGN state) and blended with Fe II lines.

Although there is a good correlation between the  $H\alpha$  and  $H\beta$  flux variability, the CCF analysis showed significantly different time delays, which are in principle connected with the BLR dimensions. It seems that the  $H\beta$  emission region is significantly larger than the  $H\alpha$  one. This should be taken with caution, since the  $H\alpha$  broad line is very sensitive to the slit offset, (see Fig. 3 and discussion in Section 2.6). I.e. a small slit offset of  $1''$  has high influence to the normalized broad  $H\alpha$  flux, but does not significantly affect the normalized  $H\beta$  flux. Therefore, the lag obtained for  $H\beta$  seems to be more relevant for discussion of the BLR dimension of around 20 light days. The He II has small time-lag (2–3 days) that is smaller than  $H\beta$ , which is usually detected in Type 1 AGNs. The obtained time-lags for He II and  $H\beta$  are in a good agreement with previous measurements, as e.g. Peterson et al. (2014) found lags of  $11.8^{+4.2}_{-2.6}$  for  $H\beta$ , and  $1.9^{+7.5}_{-1.6}$  for He II using the CCF, and  $23.6^{+1.8}_{-2.7}$  for  $H\beta$ , and  $10.4^{+2.1}_{-0.7}$  for He II using the SPEAR method (see Table 4 in their paper). I.e. both methods gave that the He II line emitting region is smaller than the  $H\beta$  one, this is in agreement with the line widths, since the He II FWHM seems to be larger than the  $H\beta$  one.

From this long-term monitoring of NGC 7469, we can conclude that the geometry of the BLR was not changed. As an illustration, in Fig. 17 we compared the mean and rms  $H\beta$

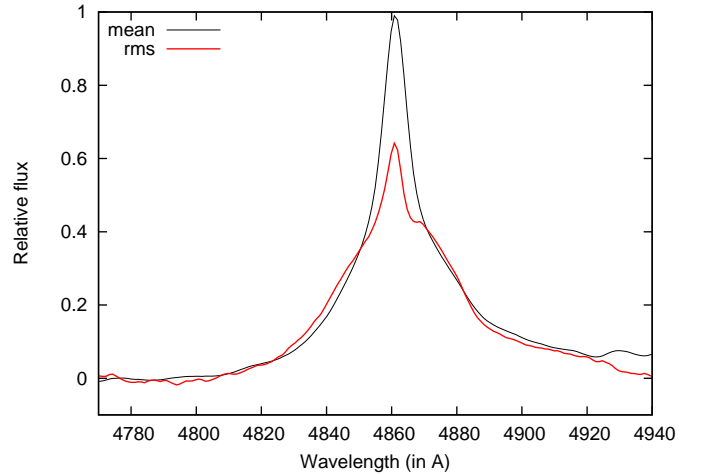


**Figure 17.** Comparison between the mean  $H\beta$  line and its rms, both profiles are normalized to the line wings.

line profiles, rescaling the rms wing intensities to the ones of the mean profile. Fig. 17 shows that the broad components are the same (there are some residuals in the centre of the rms caused by small differences in the spectral resolution). There is a slight red asymmetry, but there are no significant changes in the broad line profiles during the 20-year long monitoring period. From Gaussian fitting, shown in Fig. 8, we found that the broader Gaussian (fitting the far red wing) is shifted for about  $600 \text{ km s}^{-1}$  to the red. This asymmetry might be due to some kind of inflow, but taking that there is no changes in this (red) part of the broad line profiles during 20-year period, the inflow should be very stable or with large dimension.

## 4.2 Black hole mass

The results of the long-term monitoring can be used for the black hole mass estimation ( $M_{BH}$ ) as

$$M_{GRAV} = f \cdot M_{vir}, \quad (6)$$

$f$  is a factor that depends on the geometry of the BLR and  $M_{vir}$  is the so called "virial product" or Keplerian mass (see Collier et al. 1998; Peterson et al. 2014) that can be calculated as:

$$M_{vir} = \frac{V_{FWHM}^2 \cdot R_{BLR}}{G}, \quad (7)$$

where  $V_{FWHM}$  is the orbital velocity at that radius ( $R_{BLR}$ ) of the BLR.

We found that the lag for  $H\beta$  is around 20 days and for  $H\alpha$  around 3 days (see Section 3.2.4), the corresponding FWHMs of these two lines are  $2000 \text{ km s}^{-1}$  and  $2100 \text{ km s}^{-1}$ , respectively. The FWHMs are measured from the broad components only (see Section 3.2.1), then for the approximation of a spherical geometry in the BLR, the orbital velocity vs. FWHM relationship can be written as (see Collier et al. 1998) :

$$V = (\sqrt{3}/2) \cdot FWHM. \quad (8)$$

The orbital velocity from the  $H\beta$  FWHM is  $\sim 1700 \text{ km s}^{-1}$ , and slightly higher for  $H\alpha$ ,  $V \approx 1800 \text{ km s}^{-1}$ .



We calculated the virial product using the following relation (after including constants and unit transformations):

$$M_{\text{vir}}[M_{\odot}] \approx 0.197 \cdot V[\text{km s}^{-1}] \cdot R_{\tau}[\text{l.d.}], \quad (9)$$

where  $R_{\tau} = c\tau$  is determined from the time delays in H $\alpha$  and H $\beta$ .

The obtained virial black hole mass indicators are:  $2 \cdot 10^6 M_{\odot}$  obtained from the H $\alpha$  FWHM and time-lag and  $1.1 \cdot 10^7 M_{\odot}$  obtained from the H $\beta$  line parameters. The obtained result for H $\alpha$  is in agreement with the one given in Peterson et al. (2014), however, the obtained mass from H $\beta$  seems to be bigger than given in Collier et al. (1998); Peterson et al. (2014). This is obviously because of our estimates of the H $\beta$  BLR dimension, for which we found that is around 20 ld. However, the difference is not so big, and taking that the factor  $f$  might have value from 1. to 5.5 (Onken et al. 2004), the estimated black hole mass is around  $\sim (1 - 6) \cdot 10^7 M_{\odot}$  that is in the agreement with previously given estimates (Collier et al. 1998; Peterson et al. 2014).

## 5 CONCLUSIONS

We have presented the long-term photometric and spectroscopic monitoring campaign for NGC 7469. Previous spectral monitoring campaigns of this galaxy were shorter, and it is for the first time that the data of the 20-year long monitoring of this AGN are presented. Additionally, we present the results of the 16-year period of photometric monitoring. We measured the continuum and line fluxes (continua at 5100 Å and 6200 Å, and H $\alpha$ , H $\beta$  and He II  $\lambda 4686$  Å lines). The measured data have been analysed and different correlation between the line and continuum fluxes have been explored. We determined the time delays between the continuum and line flux variations, and at the end we used measured data for discussing the nature of the variability, the BLR structure, and to estimate the central black hole mass in NGC 7469.

Concerning our investigations of the long-term variability of NGC 7469, we can outline the following conclusions:

- (i) The AGN of NGC 7469 is surrounded by complex circumnuclear region, that may affect the observed spectra in a monitoring campaign. Our simulations show that the narrow slit observations, with relatively small offset changing (1-2'') can produce an artificial variability in the line flux, especially in the case of the H $\alpha$  line. Therefore, for future monitoring campaigns one should have this in mind.
- (ii) The long-term variability shows that the broad line and continuum fluxes of the AGN have changed for around  $F_{\text{max}}/F_{\text{min}} \sim 2$ , in the continuum and H $\alpha$  line, while in the H $\beta$  it changed for around 3 times. The changes in the He II line seem to be around 6 times. We found that in the flux variability two periods around 2600 and 1200 days may be present, however these periods have to be taken with caution since red noise may be also present. We confirm that there are several short time (1-5 days) flare-like peaks in the spectral light-curves.
- (iii) The lags of the H $\beta$  and H $\alpha$  broad lines are quite different, showing that the H $\alpha$  broad line emitting region (similar as He II) is around  $\sim 2 - 3$  light days, but H $\beta$  broad lines

is coming from a region that is ten times larger ( $\sim 20$  light days). As we noted above, the lag for H $\alpha$  should be taken with caution.

(iv) The broad line profiles did not show large change, and it seems that the emission regions are geometrically stable. The H $\beta$  and H $\alpha$  have FWHM around  $2000 \text{ km s}^{-1}$  and show a red asymmetry. This red asymmetry indicates some kind of the receding motion of the BLR emission gas with velocity of  $\sim 600 \text{ km s}^{-1}$ . It is interesting that there is no changes in the red asymmetry in the 20-year period.

We estimated the mass of the central black hole, taking the rotation velocity from the broad H $\beta$  and H $\alpha$  line FWHMs and their time delay, and found that the mass is  $\sim (1 - 6) \cdot 10^7 M_{\odot}$ , which is in an agreement with previous estimates from shorter but more intensive monitoring campaigns.

## ACKNOWLEDGEMENTS

This work was supported by: INTAS (grant N96-0328), RFBR (grants N97-02-17625 N00-02-16272, N03-02-17123, 06-02-16843, N09-02-01136, 12-02-00857a, 12-02-01237a, N15-02-02101), CONACYT research grants 39560, 54480, and 151494, and the Ministry of Education and Science of Republic of Serbia through the project Astrophysical Spectroscopy of Extragalactic Objects (176001). L. Č. P., W. K. and D. I. are grateful to the Alexander von Humboldt foundation for support in the frame of program "Research Group Linkage". W. K. is supported by the DFG Project Ko 857/32. We especially thank Borisov N.V., Fathulin T., Fioktistova I., Moiseev A., Mikhailov V. and Vlasyuk V.V. for taking part in the observations.

## REFERENCES

- Afanasiev V.L., et al., 2016 (in preparation)
- Amirkhanian V., et al., 2000, Bull. Spec. Astrophys. Obs. 50
- Anderson, K. S. 1973, ApJ, 182, 369
- Artamonov, B. P., Bruevich, V. V., Gusev, A. S., Ezhkova, O. V., Ugol'Kova, L. S., Shimanovskaya, E. V. 2010, Astronomy Reports, Volume 54, Issue 9, pp.767-775
- Baldi, R. D., Behar, E., Laor, A., Horesh, A. 2015, MNRAS, 454, 4277
- Bentz, M. C., Denney, K. D., Grier, C. 2013ApJ...767..149B
- Burbidge, E. M., Burbidge, G. R., Prendergast, K. H. 1963, ApJ, 137, 1022
- Chuvaev, K. K., Lyutyi, V. M., Doroshenko, V. T. 1990, SvAL, 16, 372
- Colina, L., Alberdi, A., Torrelles, J. M., Panagia, N., Wilson, A. S. 2001, ApJ, 553L, 19
- Colina, L., Díaz-Santos, T., Alonso-Herrero, A., Panagia, N., Alberdi, A., Torrelles, J. M., Wilson, A. S. 2007, A&A, 467, 559
- Collier, S. J., Horne, K., Kaspi, S. et al. 1998, ApJ, 500, 162
- Cousins, A.W.J., 1976, Mem.R.Astron.Soc. 81, 25
- Davies, R. I., Tacconi, L. J., Genzel, R. 2004, ApJ, 602, 148
- Díaz-Santos, T., Alonso-Herrero, A., Colina, L., Ryder, S. D., Knapen, J. H. 2007, ApJ, 661, 149
- Dietrich, M., Peterson, B. M., Albrecht, P., et al. 1998, ApJS, 115, 185
- Doroshenko, V. T., Sergeev, S. G., Merkulova, N. I., et al. 2005, Astrophysics, 48, 304

- Doroshenko, V. T., Sergeev, S. G., Vovk, E. Y., et al. 2010, *Astronomy Letters*, 36, 611
- Dultzin-Hacyan, D., Schuster, W. J., Parrao, L., Pena, J. H., Peniche, R., Benitez, E., Costero, R. 1992, *AJ*, 103, 1769
- Glass, I. S. 1998, *MNRAS*, 297, 18
- Izumi, T., Kohno, K., Aalto, S. et al. 2015, *ApJ*, 818, 42.
- Kovačević, J., Popović, L. Č. Dimitrijević, M. S., 2010, *ApJS*, 189, 15
- Kovačević, A., Popović, L. Č., Shapovalova, A. I., et al. 2014, *Advances in Space Research*, 54, 1414
- Leighly, K., Kunieda, H., Awaki, H., Tsuruta, S. 1996, *ApJ*, 463, 158
- Lyutiy, V. M., Doroshenko, V. T., Metlov, V. G., Irsmbabetova, T. R. 1995, *AstL*, 21, 581
- Marquez, I., Moles, M. 1994, *AJ*, 108, 90
- Merkulova, N. I. 2000, *AJ*, 119, 631
- Nandra, K., Clavel, J., Edelson, R. A., George, I. M., Malkan, M. A. et al. 1998, *ApJ*, 505, 594
- O'Brien, P.T., Dietrich, M., Leighly, K. et al. 1998, *ApJ*, 509, 163
- Onken, C. A., Ferrarese, L., Merritt, D., Peterson, B. M., Pogge, R. W., Vestergaard, M., Wandel, A., 2004, *ApJ*, 615, 645
- Penston, M.J., Penston, M.V., Sandage, A., 1971, *PASP* 83, 783
- Petrucci, P. O., Maraschi, L., Haardt, F., Nandra, K. 2004, *A&A*, 413, 477
- Pérez-Torres, M. A., Alberdi, A., Colina, L., Torrelles, J. M., Panagia, N., Wilson, A., Kankare, E., Mattila, S. 2009, *MNRAS*, 399, 1641.
- Peterson, B. M. 1993, *PASP*, 105, 247
- Peterson, B. M., 2014, *SSRv*, 183, 253
- Peterson, B. M., Berlind, P., Bertram, R., et al. 1994, *ApJ*, 425, 622
- Peterson, B. M., Berlind, P., Bertram, R., et al. 2002, *ApJ*, 581, 197
- Peterson, B.M., Collins II, G.W. 1983, *ApJ*, 270, 71
- Peterson, B. M., Denney, K. D., De Rosa, G. et al. 2013, *ApJ*, 779, 109
- Peterson, B. M., Grier, C. J., Horne, K., Pogge, R. W., Bentz, M. C. et al. 2014, *ApJ*, 795, 149
- Peterson, B. M., Pogge, R. W., Wanders, I., Smith, S. M., & Romanishin, W. 1995, *PASP*, 107, 579
- Peterson, B. M., Wanders, I., Bertram, R., et al. 1998, *ApJ*, 501, 82
- Popović, L. Č., Mediavilla, E., Bon, E., & Ilić, D. 2004 *A&A* 423, 909
- Pronik, I. I., 1974, *ATsir*, 831, 8
- Pronik, I. I. 1975, *AZh*, 52, 481
- Pronik, I. I. 1976, *SvA*, 19, 293
- Pronik, I. I. 2009, *A&A*, 496, 299
- Pronik, I. I., Metik, L. P., Merkulova, N. I. 1996, *Ap&SS*, 239, 97
- Pronik, I. I.; Metik, L. P.; Merkulova, N. I. 1997, *A&A*, 318, 721
- Rasmussen, C. E. and Williams, C., *Gaussian Processes for Machine Learning*, the MIT Press 2006
- Rouan, D., Gratadour, D. 2008, *JPhCS*, 131, a2035
- Shapovalova, A. I., Burenkov, A. N., Carrasco, L., et al. 2001, *A&A*, 376, 775
- Shapovalova, A.I., Doroshenko, V.T., Bochkarev, N.G, et al. 2004, *A&A*, 422, 925
- Shapovalova, A. I., Popović, L.Č., Bochkarev, N.G., et al. 2010, *A&A*, 517A, 42
- Shapovalova, A. I., Popović, L.Č., Bochkarev, N.G., et al., 2013, *A&A*, 559A, 10S
- Shapovalova, A.I., Popović, L.Č., Burenkov, A. N., et al. 2012, *ApJS*, 202, 10
- Shapovalova, A.I., Popović, L.Č., Chavushyan, V., et al. 2016, *ApJS*, 222, 25
- Shapovalova, A.I., Popović, L.Č., Collin, S., et al. 2008, *A&A*, 486, 99
- Ugol'kova, L. S., Artamonov, B. P. 2011, "Odessa Astronomical Publications, vol. 24, p. 78
- Ulrich, M.-H. J. 1972, *ApJ*, 171L, 37
- Vlasyuk V.V., 1993, *Bull. Spec. Astrophys. Obs.* 36, 107
- Wanders, I., Peterson, B. M., Alloin, D. et al. 1997, *ApJS*, 113, 69
- Wilson, A. S., Baldwin, J. A., Sun, S.-D., Wright, A. E. 1986, *ApJ*, 310, 121
- Wilson, A. S., Helfer, T. T., Haniff, C. A., Ward, M. J. 1991, *ApJ*, 381, 79
- Yankulava, I. M. 1973, *ATsir*, 769, 1

This paper has been typeset from a  $\text{\TeX}/\text{\LaTeX}$  file prepared by the author.